

Towards biaxial fatigue experiments of elastomers using square and cruciform geometries in planar tension conditions

Ali Esmaeili^a, Deepak George^a, Lewis Tunnicliffe^c, Ian Masters^a, Mokarram Hossain^{a,b,*} 

^a Zienkiewicz Institute for Modelling, Data and AI, Faculty of Science and Engineering, Swansea University, SA1 8EN, Swansea, United Kingdom

^b Materials and Manufacturing Research Institute, Faculty of Science and Engineering, Swansea University, SA1 8EN, Swansea, United Kingdom

^c Birla Carbon, 1800 West Oak Commons Court, Marietta, GA, 30062-2253, USA

ARTICLE INFO

Keywords:

Natural rubber
Ecoflex
Biaxial test
Fatigue test
Digital Image Correlation (DIC)

ABSTRACT

Soft materials such as natural rubber, hydrogels, and biological tissues have anisotropic properties and are subject to cyclic biaxial loading during their service lives. This requires biaxial loading rather than uniaxial; however, no agreed standard protocol exists. Therefore, the aim of this study is to provide preliminary suggestions for reliable and consistent biaxial fatigue tests so that a good degree of biaxiality and efficiency can be thoroughly achieved. Several biaxial loading tests (equi-biaxial and unequal-biaxial) were conducted on natural rubber and ecoflex using different geometries including cruciform and square configurations. Three criteria were defined to evaluate the equi-biaxiality performance: (i) test function related to homogeneous strain distribution in the field of interest, (ii) degree of efficiency corresponding to the ratio of strain in the field of interest (gauge section located in the middle regions) to the maximum strain far from the middle area, and (iii) strain ratio, used for fatigue test. Results showed that cruciform geometry underperformed in equi-biaxiality criteria, i.e., samples possessed high uniaxial strain in the arm whereas the simple square geometry could reach a higher degree of biaxiality and efficiency. The highest equi-biaxiality performance was obtained for the optimized square geometry in such a way that a maximum equi-biaxial strain of 65 % was achieved in the field of interest while possessing a degree of efficiency of 0.66 and strain ratio of 1.96. A successful unequal-biaxial fatigue test of up to two million cycles was conducted on the optimized square specimen made of ecoflex. Finally, a new square configuration with circular cavity in the middle was suggested for future biaxial characterization and standardization of biaxial tests in which the numerical study yielded a degree of efficiency of 1 and strain ratio of 2.12 manifesting a considerable improvement in the biaxiality performance.

1. Introduction

Understanding the mechanical performance of soft materials such as elastomers and biological tissues under cyclic conditions have been studied mostly in uniaxial conditions [1,2]. However, many of these materials manifest anisotropic characteristics especially in biological tissues [3] and rubbers compounded by the calendaring process [4]. In addition, the typical loading scenario for some applications including Wave Energy Converters (WECs) [5–7], Magneto-Rheological Elastomers (MREs) [8–10] and Dielectric Elastomers Generators (DEGs) [11] used in soft robotics and flexible sensors are mostly experiencing cyclic-biaxial rather than simple cyclic-uniaxial loadings. Therefore, evaluating biaxial fatigue performance of such materials can provide a

better insight toward material behaviour under a more realistic test condition [12].

In this context, bulge test also known as bubble or inflation test is one of the most common biaxial tests performed on rubber-like materials [13,14] in which the stress state at the apex of the dome is equi-biaxial (EB) [15]. This can be a suitable method for thin film membranes. The value of the displacement and height at the apex shall be known so that any suitable material can be characterized. However, it is less satisfactory at large strains where the thickness is not uniform in the inflated membrane during bulging [16]. In this context, performing biaxial test using square or cruciform configurations mitigate the problem (thickness variation in the inflated membrane at large strain) since the stress-strain behaviour can be obtained as the thickness is the same in

* Corresponding author. Materials and Manufacturing Research Institute, Faculty of Science and Engineering, Swansea University, SA1 8EN, Swansea, United Kingdom.

E-mail address: mokarram.hossain@swansea.ac.uk (M. Hossain).

<https://doi.org/10.1016/j.polymertesting.2025.109060>

Received 26 August 2025; Received in revised form 10 November 2025; Accepted 27 November 2025

Available online 29 November 2025

0142-9418/© 2025 The Authors. Published by Elsevier Ltd. This is an open access article under the CC BY license (<http://creativecommons.org/licenses/by/4.0/>).

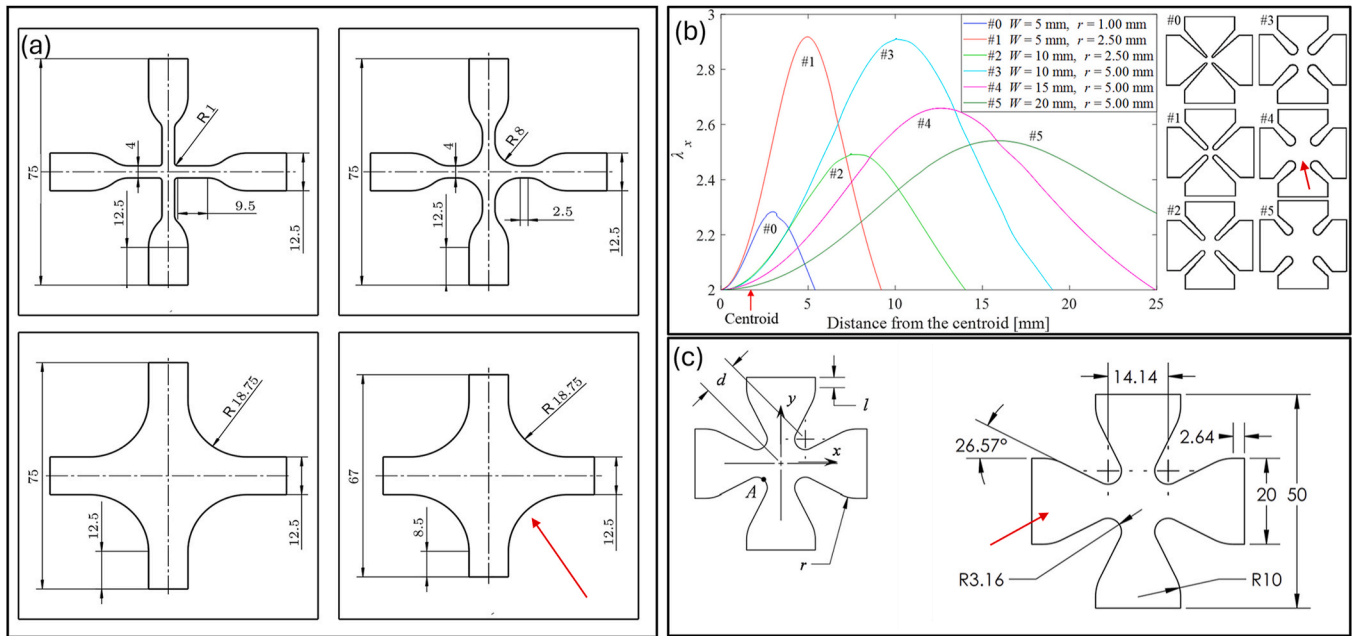


Fig. 1. Sample optimization performed on the cruciform samples: (a) silicone rubber ELASTOSILR©RT 625 [26], (b) silicone elastomer where W and r are the narrowest width of the arm and the fillet radius respectively [27], (c) magnetorheological elastomers [28]. Red arrows in each figure refer to final optimized specimen selected in each study.

the EB regions; therefore, no significant thickness variation can be seen even at high strains.

In addition, the area of the equi-biaxiality is quite small in the bulged membrane compared to other biaxial geometries where a larger area of biaxiality can be reached, for instance in square configuration [17]. The bigger area of equi-biaxiality for the cruciform and square specimens results from the flatness of the sample whereas the curvature of the membrane in the bulge test makes the EB modes only in the apex which is a small area. Furthermore, the existing membrane theories used for bulging a thin film consider trivial thickness and its subsequent shear deformation in the lateral directions which are not quite true in the real bulge test [18]. The inability to apply different loading conditions such as Unequal-biaxial (UB) or Planar Tension (PT) rather than simple EB-loading is another drawback of bulge test. On the other hand, square or cruciform configurations can provide much better flexibility applying variety of loading due to their flatness. In addition, UB tension testing on a flat sample (square or cruciform) in planar condition can be a better approach for other applications such as soft robotics, WECs as they are typically subjected to a larger area of UB loading during their service lives. Two representative WECs are the *mWave*™ developed by *Bombora Wave Power* made of rubber membranes [19,20] and the *WEC S3*® by *SBM Offshore* composed of a long flexible tube made of an Electro-active Polymer (EAP) [21]. In both cases, the typical loading condition are mostly UB and PT instead of EB.

A comprehensive review was conducted by Esmaili et al. [12] on biaxial characterizations in the planar condition in which different sample geometries and gripping systems were discussed in detail. Fig. 1 shows some of the optimizations conducted on cruciform samples made of elastomers which are the basic studies for our investigation, specifically for the definition of biaxiality criteria. The configurations marked by the red arrows in Fig. 1 are the ones selected after the optimization of each study. It can be concluded that huge discrepancies existed in terms of cruciform geometries used. The cruciform configuration marked by the red arrow in Fig. 1a is selected in this study. A few other optimized cruciform geometries were also used for composite woven fabrics which is worth implementing them [21–24] for elastomer in the future studies [22–25]. Although many studies are available on the optimization of cruciform geometry, no optimization was performed on square

Table 1

Biaxial (EB) fatigue tests using the bulge test performed on various elastomers.

Material	EB strain (%)	Maximum fatigue life (Cycle No.)	Ref
Silicone based MREs	25 %	~10000	[10, 35]
Silicone based MREs	25 %	561	[14]
70 IRHD Ethylene-Propylene rubber (EPM)	70 %	800000	[36]
EPDM rubber	110 %	2722	[37]

geometry which lack deep understanding of its performance in biaxial mode. This is one of our novelties to further extend the biaxiality criteria defined in section 4 for the square specimen and optimize the square geometry based on the biaxiality performance.

In addition, some of the fatigue tests conducted on soft materials using the bubble test are listed in Table 1 whereas no study has been reported on biaxial tension fatigue test in planar conditions. Considering the limitations of the bulge test discussed before, it is essential to develop a more robust and cost-effective biaxial fatigue testing methodology in which it can not only reach to a higher area of equi-biaxiality, but can also achieve a higher number of cycles when subject to fatigue test with no concern about premature failure resulting from the clamping system. Likewise, the new biaxial test methodology shall be flexible enough that different loading scenarios can be easily applied including UB, EB, and PT. There are very limited works on planar biaxial testing of rubber-like materials in quasi-static conditions using flat samples [29–34].

The literature still lacks a proper biaxial tension approach in planar condition to address and overcome the shortcoming of bulge test including thickness variation during the inflation, inability in applying various biaxial loading states (EB, UB, PT), its consideration of trivial thickness and subsequent shear deformation in the lateral directions. In addition, no biaxial fatigue test was reported using cruciform or square geometries.

Developing a robust way of performing biaxial tension fatigue tests, where the sample does not demonstrate premature failure resulting from

Table 2
EDS35 formation in phr.

Materials	SMR CV60	Zinc oxide	Stearic acid	6 PPD	Sasol wax	CBS	Sulphur
EDS35	100	5	2	3	2	1.5	1.5

the stress concentration imposed by the clamping system or poor test design, is the gap of knowledge in the field. Currently, performing a high cyclic biaxial fatigue test in planar conditions is not very feasible due to aforementioned issues, thus, it is not possible to thoroughly evaluate biaxial fatigue life in an elastomer which is an inherent property and should not be dependent on test design or experimental setup. Recognised difficulties in conducting proper planar biaxial tests due to restrictions arising from sample geometry, degree of biaxiality in the Field of Interest (FOI) and gripping challenges led to optimization of the sample geometries used in the current study. Therefore, this paper is aimed at providing some preliminary insights in performing biaxial tension fatigue tests and to achieve high cyclic biaxial fatigue data through the optimization of the test coupon by enhancing its mechanical properties in the gripping area eliminating premature failure arising from stress concentration imposed by grips.

Given this background information, various biaxial fatigue states are investigated in the current study using cruciform and square configurations including EB and UB modes, although the main focus of this paper is to successfully perform high cyclic UB fatigue tests where the strains in longitudinal and transverse directions are approximately 45–55 % and 5–10 %, respectively, to mimic service condition of the innovated WEC S3® membrane technology developed by *SBM Offshore* [21]. Extensive comparisons of various biaxial tests possessing relatively similar testing conditions will be performed in this study: (i) to compare the degree of biaxiality and degree of efficiency in the FOI in the case of EB test, (ii) to obtain 2D strain fields which can be used to attain the degree of biaxiality and efficiency.

The outcome of this paper can be applied for any soft polymers such as biological materials and tissues where biaxial characterization is of great importance. Since there is no established test protocol for biaxial planar tension fatigue, the findings presented here including sample configurations, customized biaxial fatigue machine used, and gripping

system design can be a potential standardized test procedure.

2. Materials and methodology

2.1. Materials

Two different materials including natural rubber (EDS35) and silicon rubber *Ecoflex*™ 00–30 that is a platinum-catalyzed silicones purchased from *SMOOTH-ON*, were used. EDS35 formulation is listed in Table 2. Zinc oxide, stearic acid, 6 PPD and Sasol Wax were incorporated into natural rubber SMR CV60 by internal mixer whereas sulphur and CBS, as curative, were added on the two-roll mill.

2.2. Samples preparation

Fig. 2 shows the NR compounding steps used in this study. Readers are advised to refer to our previous study [38] for further information about compounding and mixing. Rheometric characterization was performed to find out vulcanization parameters. Uncured rubber was tested at temperatures of 150 °C (Fig. 2h) and subsequently samples were compression moulded with the dimension of 9" x 9" x 2 mm at 150 °C for 15 min based on the torque-time curve obtained from the rheometric test.

Three different geometries were employed in the current study as shown in Fig. 3. This is to further investigate the effect of various geometries in equi-biaxiality performance and to compare their fatigue lives. In addition, this helps to put more efforts toward optimization of the samples to be used in tension biaxial testing where lack of standards for biaxial characterization of elastomers still exist. Finally, by comparing various configurations in the tension biaxial mode, a more effective and robust sample configuration in terms of the gripping effect imposed on the samples throughout the test can be identified. The optimized cruciform specimen suggested by Seibert et al. [26] with dimensions shown in Fig. 3a were used in this study. NR cruciform samples were prepared with a die cutter shown in Fig. 3b.

The second geometry used in this study was a reinforced square sample with a reduced gauge section (thickness) in the middle based on the approach used in Refs. [40,41]. The gauge section of the specimen was as thin as 0.8 mm while the edges were reinforced by increasing

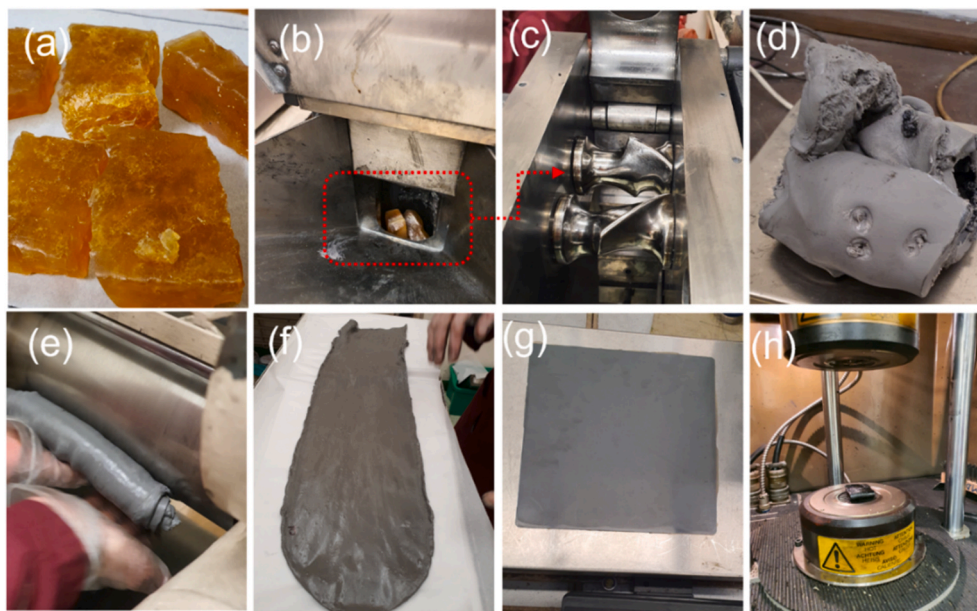


Fig. 2. EDS35 compounding steps: (a) SMR CV60 gum [39], (b) initial mixing of NR gum in the internal mixer, (c) close-up view of the internal mixer, (d) dumped compound including NR-zinc oxide-stearic acid- 6 PPD- Sasol Wax, right after mixing by internal mixer, (e) adding sulphur and CBS and further mixing and homogenization by two-roll mill, (f) unvulcanised rubber containing all ingredients, (g) vulcanised rubber right after compression moulding, (h) Rheometry.

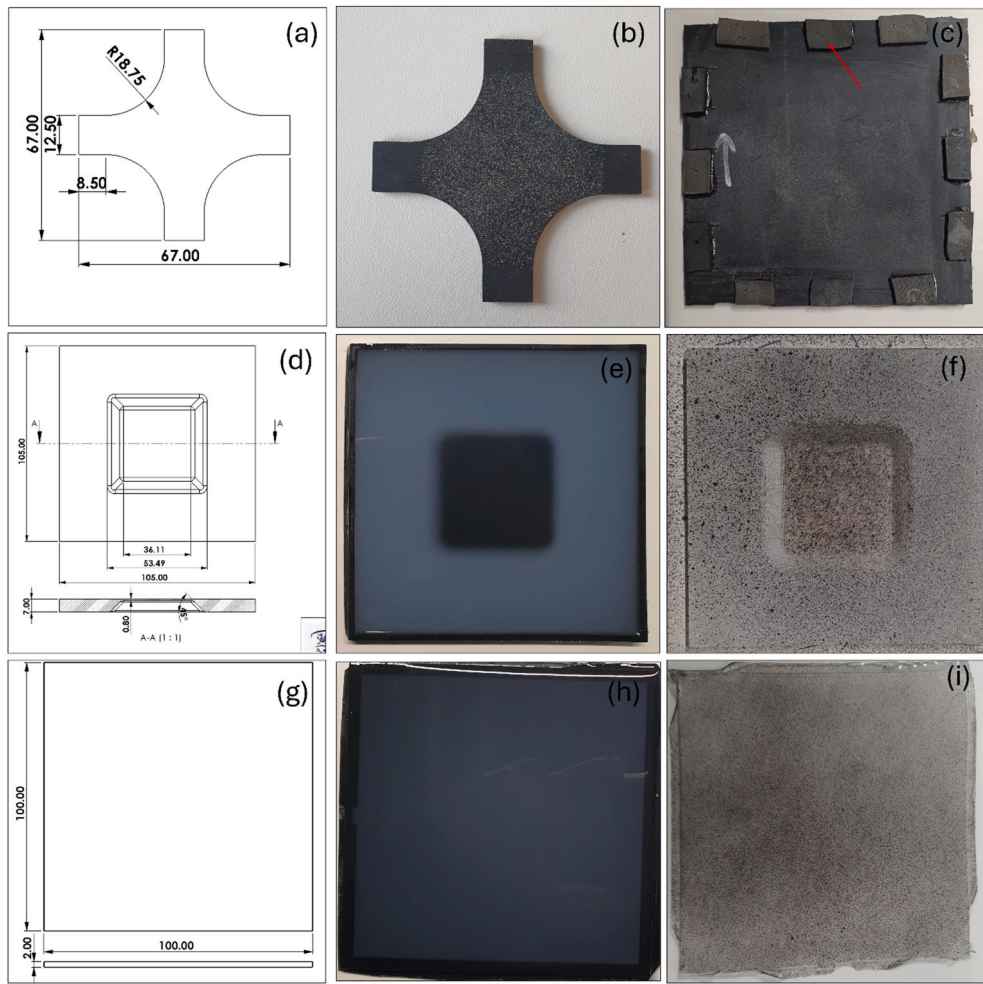


Fig. 3. Specimen configurations: (a) NR cruciform geometry, (b) NR die cutter-cruciform sample, (c) NR edge-reinforced simple square. (d) Ecoflex optimized square specimen, (e) moulding and curing of ecoflex optimized sample in the 3D printed mould, (f) ecoflex optimized sample upon moulding and speckled with black spray paint, (g) ecoflex simple square, (h) moulding of ecoflex simple square sample in the 3D printed mould, (i) ecoflex simple square sample upon moulding and speckled with black spray paint.

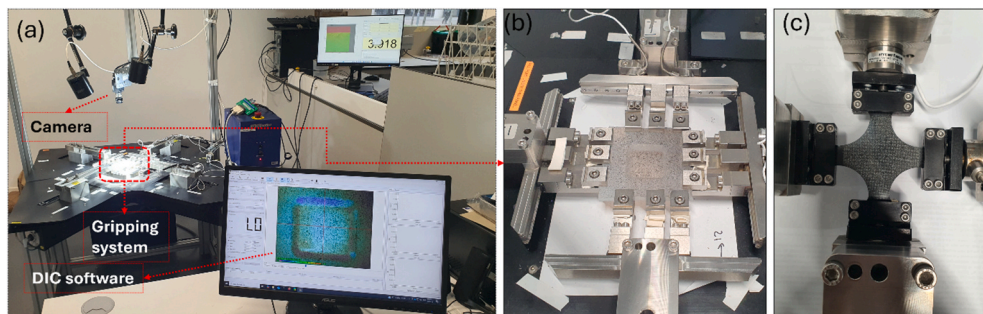


Fig. 4. Mechanical test setup: (a) biaxial fatigue test setup showing camera position and strobes, (b) sliding fingering gripping systems used for the square sample, (c) grip used for the cruciform geometry.

their thickness up to 7 mm (Fig. 3d and f). This can help to further postpone damage initiation in the vicinity of the grips so that a higher fatigue life can be achieved.

The third geometry is a more usual approach of square samples called simple square specimen (Fig. 3c). The clamping sections of the NR square coupons were reinforced by gluing extra piece of NR, as shown by red arrow in Fig. 3c. These were compared to find out which one can achieve a reliable fatigue life, create a good degree of biaxiality and survive approximately one million cycles without failure at the grips.

A DLP-based 3D printer with *BAS ST 45 B 1000* resin was used for the 3D printing of the mould. Ecoflex™ were mixed by weight ratio of 1 A:1 B and poured into the mould and left for final curing at room temperature for 3 h (Fig. 3e–f and h–i). The gauge section of the ecoflex optimized square specimen was 0.8 mm. A simple square sample made of ecoflex with 2 mm thickness was also prepared for comparison as shown in Fig. 3g–i. The surface of the samples was sprayed with *Ambersil 400* ml RAL 9011 matt spray paint for Digital Image Correlation (DIC) analysis as shown in Fig. 3b–f and i.

2.3. Biaxial testing

A highly advanced and custom-built electromechanical fatigue testing machine, *ADMET eXpert 8000, USA* was used (Fig. 4a) for all biaxial fatigue experiments. A lateral sliding pinching grip system was employed for the square geometries (Fig. 4b) such that gripping fingers on the corners can translate perpendicular to the direction of force as the material expands or contracts. A simpler grip used for the cruciform specimen is shown in Fig. 4c.

Sinusoidal displacement waveforms with 1.0 and 2.0 Hz frequencies were used for the EB and UB fatigue tests whereas a low frequency cyclic test (sinusoidal waveform) with the period of 6 s was used for the EB investigation of ecoflex-optimized squared specimen. Samples were subjected to a variety of EB and UB tests with different strain amplitudes. Test parameters including frequency and displacement amplitude of the machine are provided along with the results for each tested sample in section 5. A positive R ratio (minimum to maximum strains) via equation (1), was applied for fatigue tests to hamper rubber chains relaxation as well as occurrence of strain induced crystallites in the crack tip region, thus, a higher fatigue life can be achieved [42].

$$R_{ratio}^x = \frac{e_{xx}^{(x,y)min}}{e_{xx}^{(x,y)max}} \quad \text{and} \quad R_{ratio}^y = \frac{e_{yy}^{(x,y)min}}{e_{yy}^{(x,y)max}} \quad (1)$$

where R_{ratio}^x and R_{ratio}^y are R-ratios in X and Y-directions, respectively, $e_{xx}^{(x,y)min}$ and $e_{yy}^{(x,y)min}$ the minimum strains in X and Y-directions, respectively, and $e_{xx}^{(x,y)max}$ and $e_{yy}^{(x,y)max}$ are the maximum strains in X and Y-directions, respectively.

The biaxial machine was equipped with a 5.0 Megapixel digital camera (2448 × 2028 @ 75 fps) and a 2D DIC System analysis software. DIC were used to attain the 2D strain fields (nominal strains and maximum principal strains) and degrees of biaxiality and to show whether homogeneous strain distribution can be achieved in the case of EB test. A virtual extensometer was placed in parallel to X and Y directions to extract the nominal strain on each direction in the FOI.

The nominal stress in the FOI was calculated by force reading in each direction divided by the area (grip to grip) in the case of simple square geometry whereas FEM simulation was used to calculate the stress in cruciform and optimized square samples as explained in Section 3. Hereinafter forces 1 and 2 and displacements 1 and 2 correspond to the Y and X directions, respectively.

It is worth noting that the high cyclic UB fatigue test conducted in this study is aimed to mimic service condition of flexible membrane used in WECs [21] such that an UB fatigue test, 45–55 % and 5–10 % strains in Y and X directions, respectively, can be thoroughly performed on square samples. High cyclic EB fatigue tests were also conducted on NR-cruciform and NR-simple square to provide better insight toward EB biaxial fatigue tests. Fatigue life was considered as the number of cycles to complete failure, however, the damage initiation should take place away from the influence of the grip for a test to be considered reliable.

3. Numerical modelling

The main objective of this section is to understand the behaviour of different biaxial test geometries. For this, we compare simulation results from various biaxial geometries to that of the Treloar's data [43]. Firstly, simulation of the inflation experiment conducted by Treloar [43] is performed to establish the adequacy of the nonlinear constitutive model selected for the study. Later, different biaxial test geometries are simulated to plot the stress-strain behaviour of the same material and is compared to the results from the inflation test.

The phenomenological model proposed by Carroll [44] is used to model the constitutive behaviour of the material. The model better suits the biaxial behaviour of polymers with minimum variation in uniaxial extension as illustrated by Ref. [45]. Carroll model takes the following

Table 3

Constitutive parameters for the NR chosen in this study [45].

a (MPa)	b (MPa)	c (MPa)	K (MPa)
0.1988	3.141e−7	2.2e−14	198.8

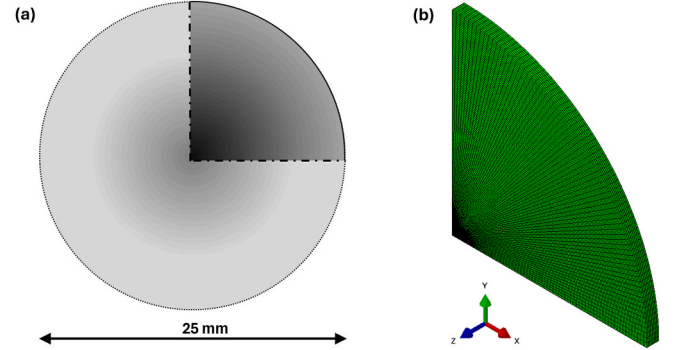


Fig. 5. (a) Circular NR membrane with 25 mm diameter and 0.8 mm thickness in plan showing a quarter for symmetry used for modelling, (b) meshing the quarter of the membrane inflation problem modelled using C3D8H elements in ABAQUS.

form (equation (2)) in which the isochoric part of the strain energy density function is given by:

$$\Psi_{iso} = a\bar{I}_1 + b(\bar{I}_1)^4 + c\sqrt{\bar{I}_2} \quad (2)$$

where, a , b and c are constitutive parameters and \bar{I}_1 and \bar{I}_2 are the isochoric strain invariants. The total strain energy density function is obtained by adding a volumetric contribution defined by equation (3):

$$\Psi_{vol} = \frac{K}{2}(J - 1)^2 \quad (3)$$

where, K is the bulk modulus of the material and J is the Jacobian defined as $J = \det(\mathbf{F})$ and \mathbf{F} is the deformation gradient tensor. The values of constitutive parameters are chosen as given in Ref. [45] for NR where they are calibrated against Treloar's data and are listed in Table 3.

The bulk modulus K is chosen such that the initial Poisson's ratio is 0.4995 which represents the near-incompressibility of rubber-like materials [46]. The constitutive model is implemented in the UHYPER user subroutine of Abaqus software [47]. A quarter of the circular membrane with symmetric boundary conditions are modelled in ABAQUS using the C3D8H elements which incorporates a hybrid formulation to model the behaviour of nearly incompressible materials. Further, the path following arc-length method which is available in ABAQUS is used to simulate the membrane inflation until the final instability. Fig. 5 illustrates the geometry of the model and the meshing used in the study where a total of 81200 C3D8H elements are used.

Fig. 6 illustrates the displacement diagram where the contour values represent the vertical displacement of the membrane from the simulation at different instances of inflation of the balloon. The last image illustrates the final inflated position corresponding to a vertical pole displacement of 35.963 mm before instability.

Fig. 7 illustrates the results from the simulation, where dotted line corresponds to the experimental results obtained by Treloar and solid lines correspond to the simulation results. Fig. 7a shows the internal pressure vs strain diagram. Fig. 7b illustrates the stress vs strain relation where the simulation results are plotted against seven different extensometer lengths $L_G \in [4, 8, 12, 20, 24, 28, 40]$ mm. Here extensometer represents a virtual one corresponding to different lengths which are placed symmetric about the pole of the inflated balloon. While the experimental results correspond to 2 mm extensometer length [43], the

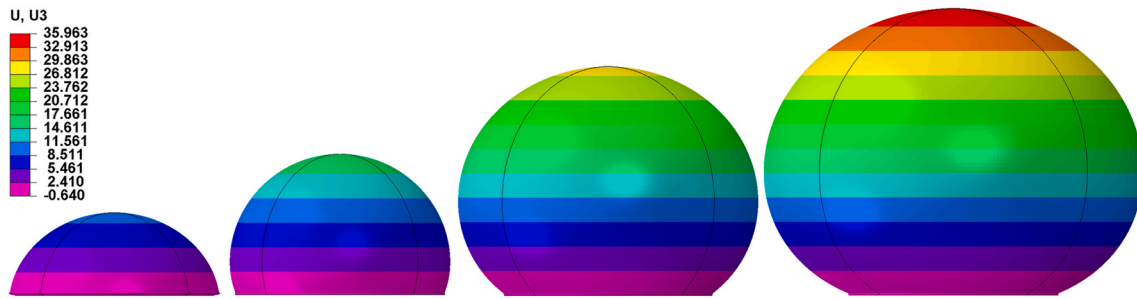


Fig. 6. Displacement diagram obtained from the simulation of the bubble test conducted by Treloar. The contour values represent the vertical displacement of the membrane represented in [mm].

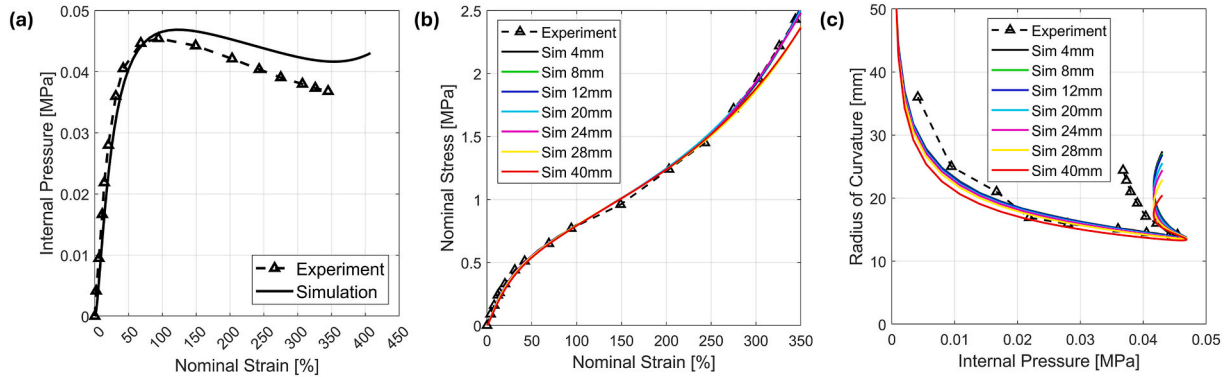


Fig. 7. Simulation results of the bubble test: (a) the internal pressure vs nominal strain at the pole for the simulation, (b) the stress-strain response of the material from EB stretching while the simulation results are presented for seven different extensometer lengths of 4, 8, 12, 20, 24, 28, 40 mm, (c) the radius of curvature vs internal pressure. In all the diagrams, dotted lines correspond to the result of experiments conducted by Treloar [43] and the solid lines correspond to the results from the simulation.

simulation show identical results for all the extensometers. This is due to the near identical curvature values of the inflated membrane over varied lengths about the pole. The internal pressure for a membrane inflation problem can be approximated using the following equation (equation (4)):

$$p = \frac{2T}{r} \quad (4)$$

where p is the internal pressure [MPa], T is the tension per unit length of the membrane [N/mm] and r is the radius of curvature of the polar region of the inflated membrane [mm]. The nominal stress P in the membrane is obtained by following equation (equation (5)):

$$P = \frac{pr\lambda}{2t} \quad (5)$$

where, t is the initial thickness of the membrane [mm] and λ is the stretch calculated from the nominal strain 'e' in either planar X or Y directions as given in equation 6

$$\lambda = (1 + e) \quad (6)$$

The nominal stress calculated in Fig. 7b corresponds to different extensometer lengths and the corresponding calculated curvature values based on the deformed coordinates of the nodes covered by the extensometer. The nominal strain 'e' is calculated based on the change in length of the virtual extensometer which becomes curved while inflated. Finally, Fig. 7c illustrates the relation between the radius of curvature and the internal pressure of the membrane. Here, different solid lines denote different lengths symmetric about the pole, which are used to calculate the radius of curvature. For the ease of calculation of nominal stress, the lengths used in curvature calculation are kept the same as that of the extensometer lengths discussed in Fig. 7b. Overall, the simulation

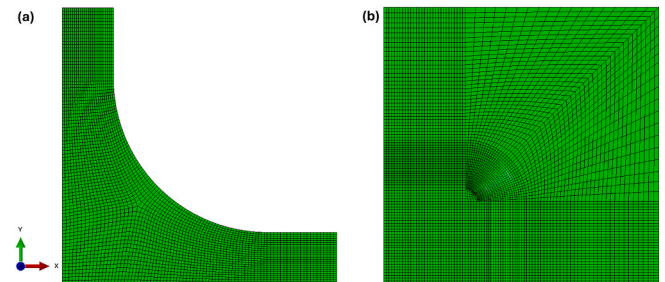


Fig. 8. Meshing of specimens: (a) cruciform, (b) optimized square geometry.

results suggest that all extensometer lengths result in a nearly identical radius values while closely following the experimental results. This illustrates the effectiveness of the constitutive model used in the study.

We extended this simulation to cruciform and optimized square configurations to further validate our numerical model in planar condition using the same material properties listed in Table 3. Fig. 8 shows the meshing of both geometries wherein, a quarter of the geometry is modelled using symmetry boundary conditions. The stress-strain curves obtained from the simulation are compared to that from the inflation experiment to identify the optimum extensometer length suitable for each geometry. Here the stress calculation is based on the internal reaction forces from the nodes covering the extensometer length under consideration. Similarly, the strain is calculated based on the displacement of the nodes on both ends of the extensometer considered. This method of stress calculation is widely used in the literature especially in the case where a nonuniform stress distribution in the sample is present [23,40,48–50].

Fig. 9a represents the stress-strain curves from the cruciform sample

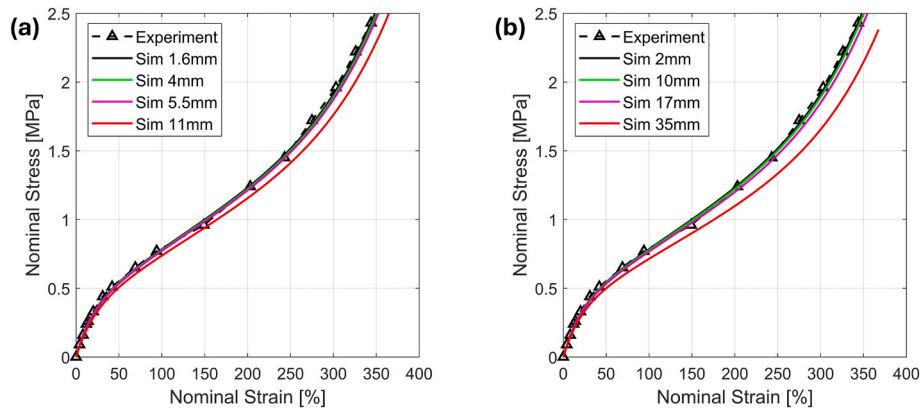


Fig. 9. Stress-strain curves corresponding to various extensometer lengths: (a) cruciform , (b) optimized square geometries.

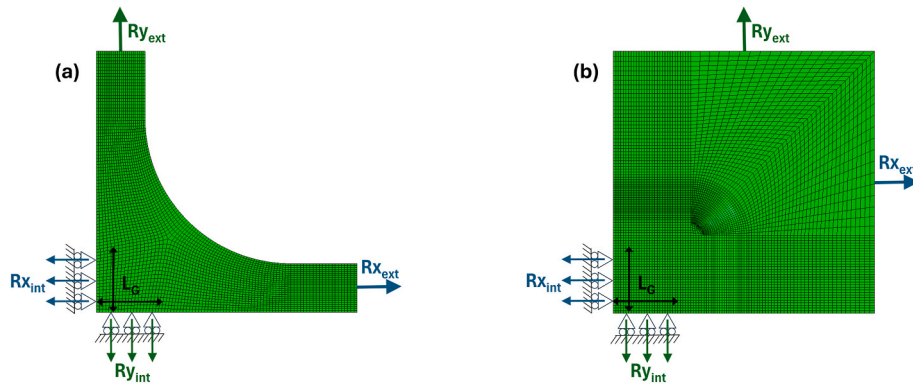


Fig. 10. ABAQUS model showing a sketch of the gauge section and the internal reaction forces for: (a) cruciform geometry, (b) optimized square geometry.

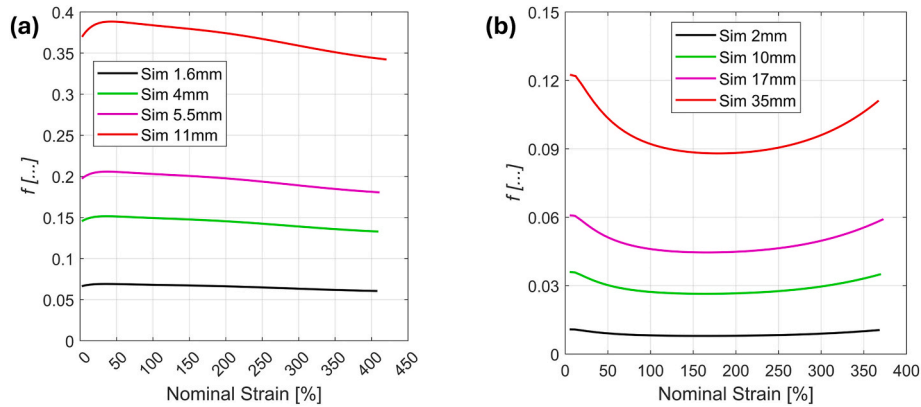


Fig. 11. Illustration of the variation of ratio 'f' at different strains corresponding to four cases of gauge length: (a) cruciform geometry, (b) optimized square geometry.

corresponding to four different extensometers $L_G \in [1.6, 4, 5.5, 11]$ mm. It can be observed that as the extensometer length reduces, the stress-strain response converges to the experimental value and a sufficient convergence can be observed for 5.5 mm long extensometer. However, for the optimized square geometry as in Fig. 9b, the response can be observed to converge for the extensometer length of 17 mm.

No variations can be seen in the stress-strain curves for various extensometer lengths up to 5.5 mm and 17 mm in cruciform and optimized square geometries, respectively (Fig. 9). Thus, the FOI of 5.5 mm and 17 mm are used to calculate the stress. However, to calculate the stresses from experiment, we also need to define a scaling parameter which will be used to calculate the internal reaction forces (in the FOI

covered by the extensometer) as a factor of the external applied force. The scaling parameter f is defined based on equation (7):

$$f = \frac{Ry_{int}}{Ry_{ext}} = \frac{Rx_{int}}{Rx_{ext}} \quad (7)$$

where, Ry_{int} and Rx_{int} are the internal reaction forces corresponding to the gauge length L_G and Ry_{ext} and Rx_{ext} are the external reaction forces in X and Y directions, respectively as shown in Fig. 10.

Fig. 11 shows the calculated values of ratio f as a function of nominal strain corresponding to gauge lengths of $L_G \in [1.6, 4, 5.5, 11]$ mm and $L_G \in [2, 10, 17, 35]$ for cruciform and optimized squares configurations, respectively. The ratio 'f' illustrates a nonlinear behaviour with respect

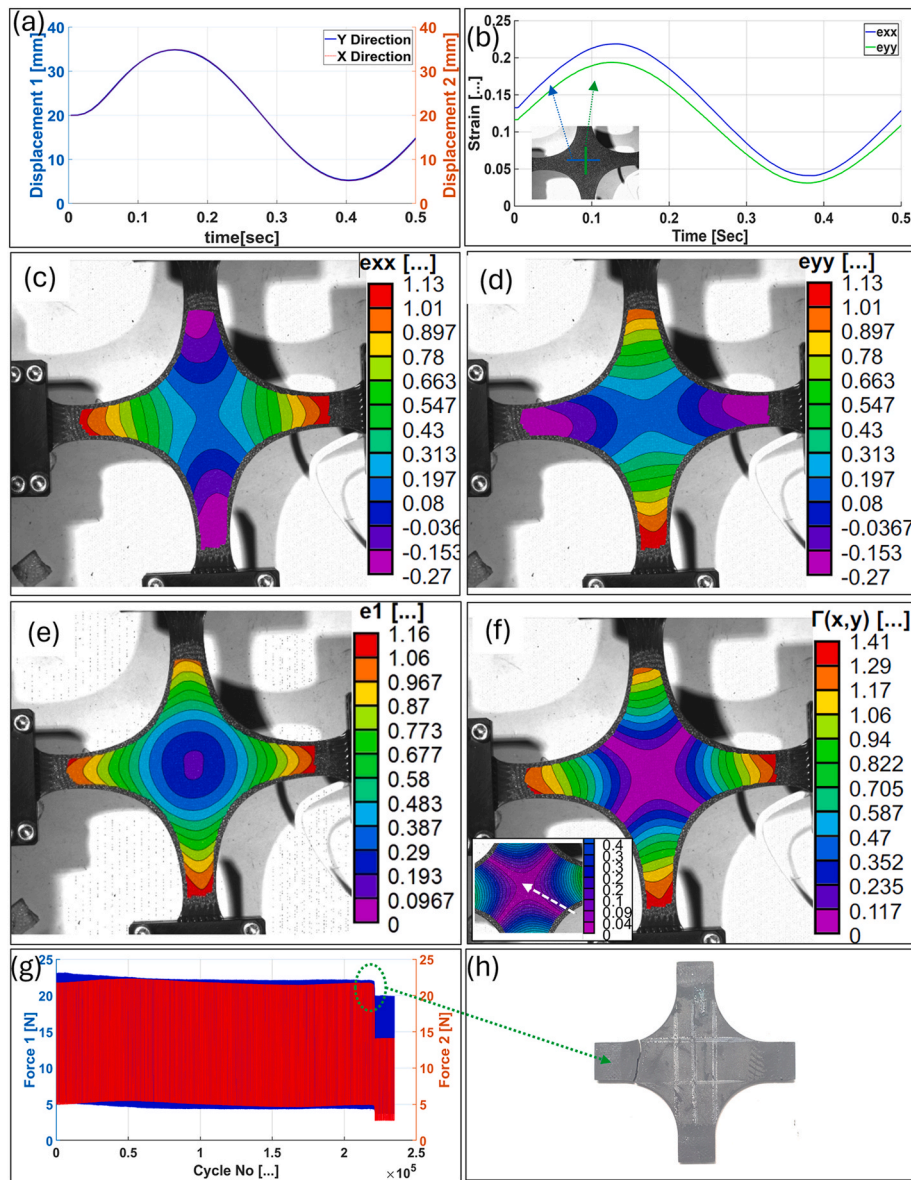


Fig. 12. EB fatigue test performed on NR-cruciform specimen: (a) displacement control parameters, (b) nominal strains over the virtual extensometers length i.e. in the FOI, (c–d) $e_{xx}^{(x,y)}$ and $e_{yy}^{(x,y)}$ distributions, respectively, at maximum displacement, (e) principal strain, e_1 , at maximum displacement, (f) $\Gamma(x,y)$ at maximum displacement while inset figure depicts area possessing test function less than 0.04 as marked by white arrow, (g) forces 1 & 2 versus number of cycles manifesting EB fatigue life of 220 K at $e_{xx}^{(x,y)} \sim 20\%$ and $e_{yy}^{(x,y)} \sim 20\%$, (h) fracture surface.

to strain. Even though the variation in the magnitude of f is negligible for the extensometer under consideration, we still resort to use the actual value of f as a function of the strain instead of a constant value [23,40,41,48–51].

Hence the nominal stress $P_{y,x}$ in either planar X or Y directions from experiment at a given strain level e in the corresponding direction is calculated using equation (8):

$$P_{y,x}(e) = \frac{f(e) \times R_y \cdot x_{ext}(e)}{L_G \times t} \quad (8)$$

where, t is the initial thickness of the sample in the gauge portion [mm].

4. Terminologies for biaxiality

There are huge discrepancies in the literature in terms of specimen geometries used for biaxial tension test in planar mode due to lack of standard or protocol [52]. Nevertheless, there is a preliminary ISO-FDIS

16842 standard on the biaxial characterization of metallic sheet in which a cruciform sample with slit in the arm was recommended [53]. Some criteria shall be met to achieve a proper grade of biaxiality [26] (in the case of EB tension test) including:

- (i) **test function ($\Gamma(x,y)$):** it indicates whether uniform and homogeneous strain can be achieved in the FOI where $e_{xx}^{(x,y)}$ and $e_{yy}^{(x,y)}$ are nominal strains in X and Y directions, respectively (equation (9)). It can be concluded that the higher the test function the higher the uniaxiality. In this paper, a test function of 0.04 are considered for proper biaxiality.

$$\Gamma(x,y) = \left| e_{xx}^{(x,y)} - e_{yy}^{(x,y)} \right| \quad (9)$$

- (ii) **degree of efficiency (η):** due to complexity of biaxial loading, uniaxial strain in the arm (for the cruciform sample) and in the

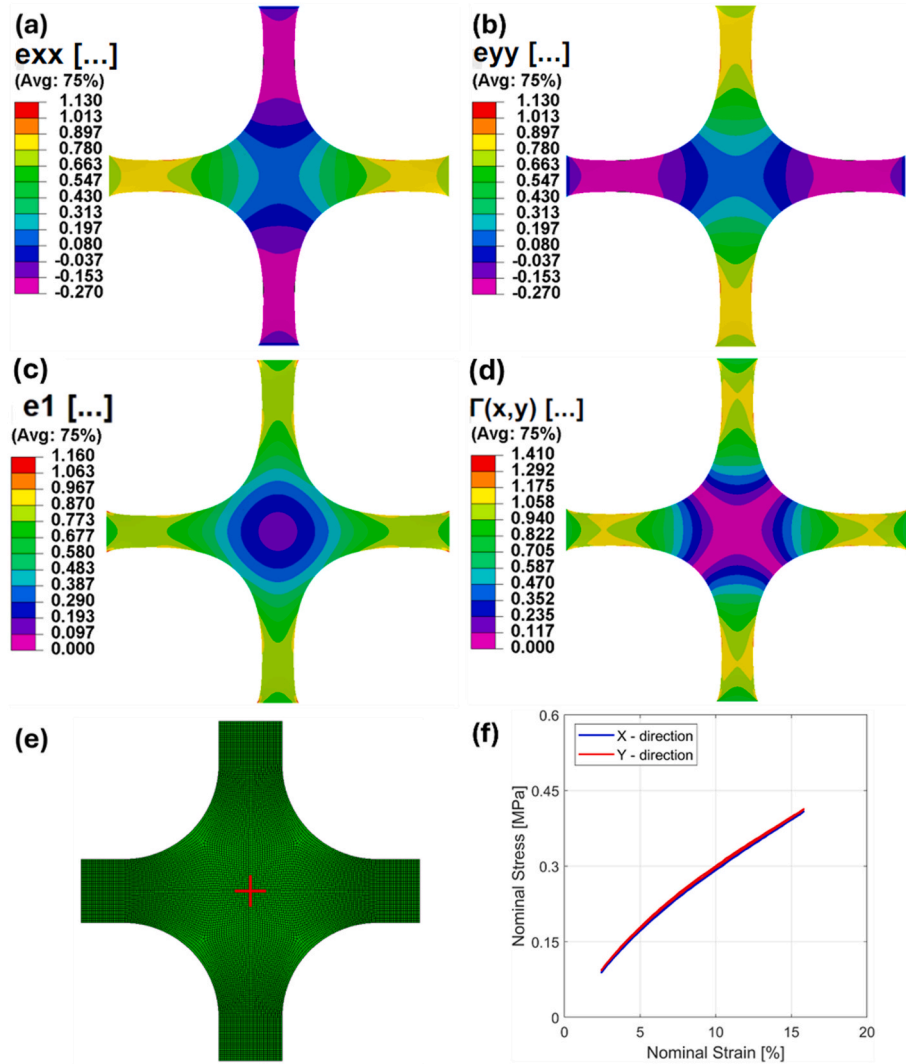


Fig. 13. Simulation results for EB tension test: (a) nominal strain in X direction, (b) nominal strain in Y direction, (c) test function $\Gamma(x,y)$ (d) maximum principal strain (e) mesh diagram showing the extensometers in red colour, (f) stress strain response corresponding to the extensometer shown in (e) possessing 5.5. Mm length.

vicinity of the grip for the square specimen are much larger than the uniaxial strain in the FOI, i.e., $e_{xx}^{(x,y)} \gg e_{xx}^{FOI}$ and $e_{yy}^{(x,y)} \gg e_{yy}^{FOI}$. This leads to improper biaxial test as the sample probably fails from the uniaxial regions instead of the FOI. Therefore, a new parameter is defined (equation (10)) to identify the amount of uniaxiality in each direction. The higher the degree of efficiency, the higher the biaxiality,

$$\eta_x = \frac{e_{xx}^{FOI}}{e_{xx}^{max}} \quad (10)$$

5. Results and discussion

5.1. NR-cruciform: EB fatigue test

Fig. 12 shows EB fatigue test parameters, nominal strains over the extensometers length in the FOI, strain distribution and EB fatigue test results performed on the NR-cruciform geometry. The displacement range of the machine is shown in Fig. 12a while the resultant strains obtained by virtual extensometer in the FOI are shown in Fig. 12b. The strain extraction in the middle of the sample was obtained by placing two virtual extensometers as shown in the inset picture in Fig. 12b.

To better interpret the strain fields, 2D contour plots of $e_{xx}^{(x,y)}$, $e_{yy}^{(x,y)}$, e_1

and $\Gamma(x,y)$ (maximum principal strain) are shown in Fig. 12c–f, respectively. The $e_{xx}^{(x,y)}$ and $e_{yy}^{(x,y)}$ are minimum in the FOI and increase uniaxially toward the arms which can be attributed to stress concentration imposed by the grip (Fig. 12c and d). Maximum principal strain (e_1) is shown in Fig. 12e manifesting its maximum values in the vicinity of the arm. A large area of biaxiality ($\Gamma(x,y) < 0.04$) is achieved as shown by white arrow in the inset of Fig. 12f. In addition, the degree of efficiency (η) is another factor that shall be met for a better biaxiality.

$$\eta_x = \frac{e_{xx}^{FOI}}{e_{xx}^{max}} = \frac{0.19}{1.13} \approx 0.17$$

Same value is obtained for η_y due to symmetry of the geometry. A maximum EB tension fatigue life of 220 K cycles (Fig. 12g) is achieved. Considering the value of degree of efficiency and e_1 , it can be concluded that the cruciform sample would fail in the vicinity of the gripping regions as shown in Fig. 12h. Therefore, a further edge enhancement shall be made on the sample. In other words, it should be further optimized by thickening the edges requiring an expensive mould. So, no further test was performed on the cruciform sample in this study.

Similar observations can be made from the simulation results presented in Fig. 13, where Fig. 13a–b and c illustrate the nominal strain in X and Y directions and the maximum principal strain, respectively. It can be observed that the simulation results for strain follow closely to that of

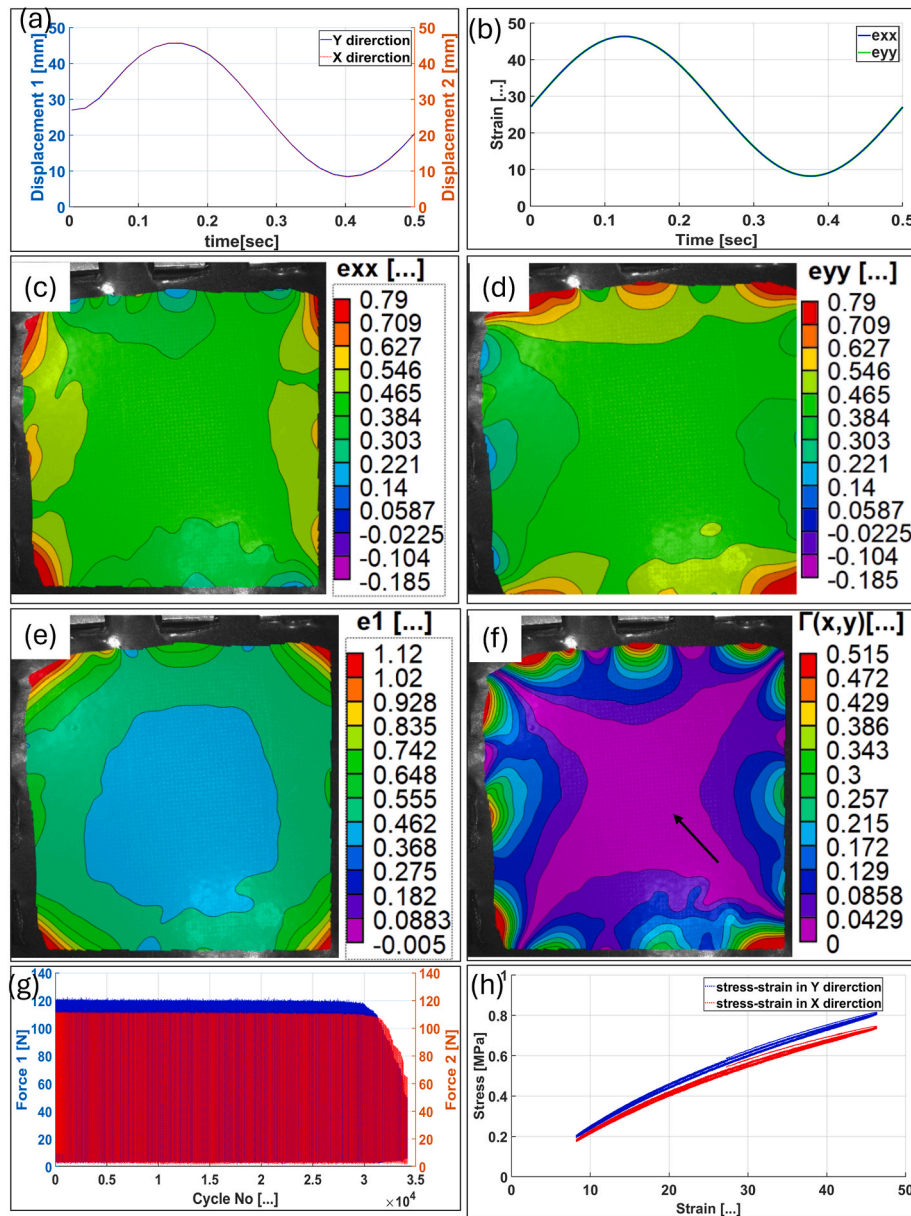


Fig. 14. EB fatigue test at 43 % strain: (a) displacement control test parameters, (b) nominal strains, (c–d) $e_{xx}^{(x,y)}$ and $e_{yy}^{(x,y)}$ fields, respectively, at maximum displacement of the machine, (e) maximum principal strain, (f) $\Gamma(x,y)$ at the maximum displacement of the machine manifesting quite large EB region in the middle, (g) force 1(Y-direction) & 2 (X-direction) versus cycle numbers manifesting EB fatigue life of 34 K at $e_{xx}^{(x,y)}$: 45 % and $e_{yy}^{(x,y)}$: 45 % (h) stress-strain curves obtained from experiment.

the experiments while there is an underprediction of the strain values in the arms. The experiment shows a maximum nominal strain value of 1.13 in the arms while the simulation results suggest a value of 0.9. This can be due to the complications arising from the gripping in the arms, resulting in an increased strain demand in the vicinity of the clamps which is not accounted in the simulation. Nevertheless, the nominal strain values in the FOI matches closely with experiments. Fig. 13d illustrates the test function $\Gamma(x,y)$, which is a good prediction of the experimental results. Fig. 13e illustrates the FOI of the cruciform sample marked by two extensometers in red colour possessing 5.5 mm length. Finally, Fig. 13f shows the stress strain diagram obtained from the experiment using the methodology described in section 3 and ratio parameters explained in Fig. 11a.

5.2. NR-simple square

5.2.1. EB fatigue test

To better understand the degree of biaxiality in the simple square specimen, a low frequency EB tension test at strain of $\sim 43\%$ was conducted only for a few cycles (Fig. 14). The displacement parameters and its consequences on imposed strains in both directions are shown in Fig. 14a and b respectively. The $e_{xx}^{(x,y)}$, $e_{yy}^{(x,y)}$, e_1 and $\Gamma(x,y)$ are presented in Fig. 14c–f, respectively. A uniform strain distribution ($\sim 42\%$) in X and Y directions can be seen in the FOI as shown in Fig. 14c and d whereas a maximum strain of 78 % can be seen near the grip. This can be further validated by the maximum principal strain in the vicinity of the grip as shown in Fig. 14e.

Unlike the cruciform sample, the area of EB region and the degree of biaxiality in the FOI is much better in the simple square geometry (Fig. 14f). In fact, the value of the test function in the FOI, corresponding

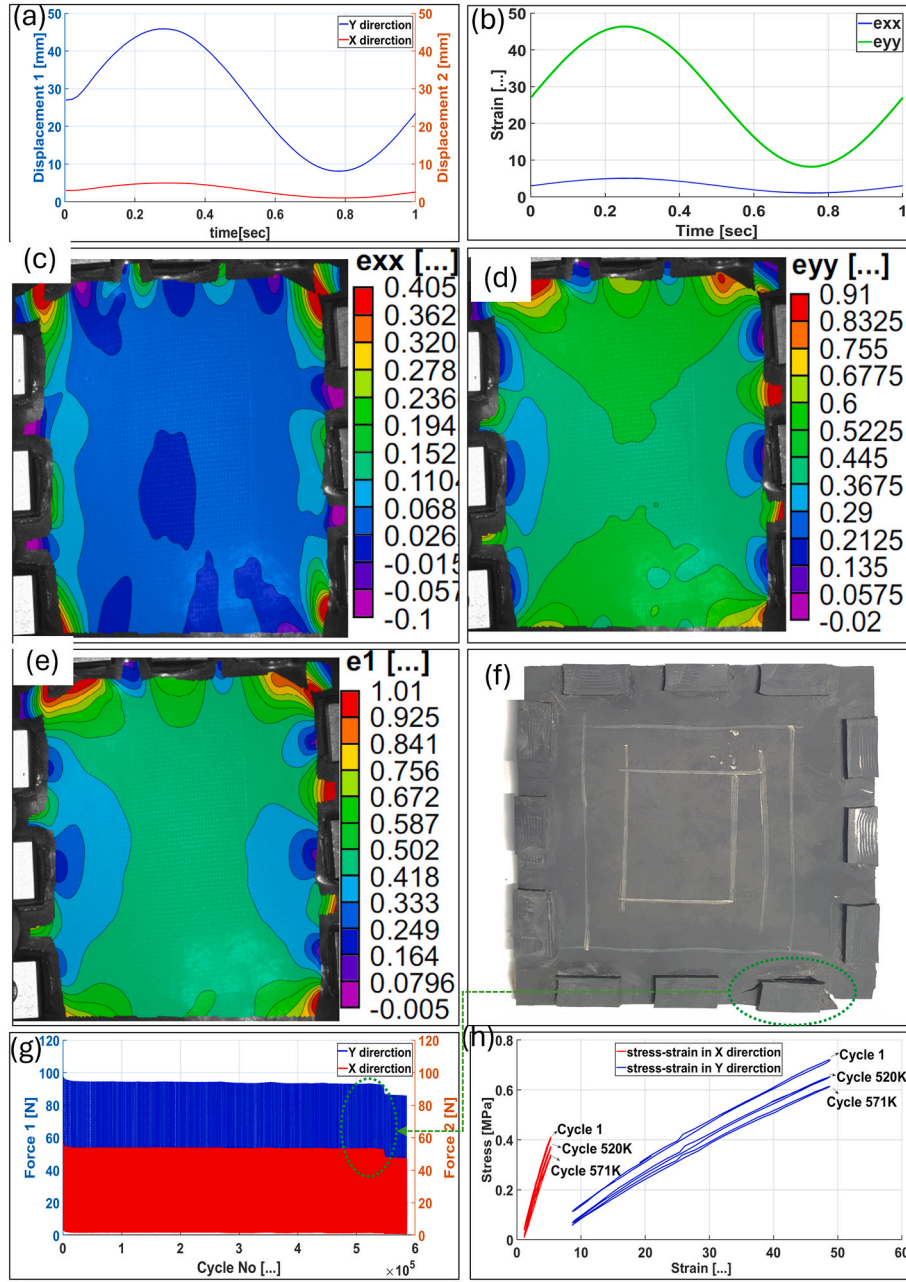


Fig. 15. UB fatigue test performed on NR-simple square specimen: (a) displacement control test parameters, (b) nominal strains, (c–d) $e_{xx}^{(x,y)}$ and $e_{yy}^{(x,y)}$ distributions, respectively, corresponding to the maximum displacement of machine, (e) maximum principal strain, e_1 , at maximum displacement (f) fracture surface, (g) force 1 (Y-direction) and 2 (X-direction) versus cycles manifesting UB fatigue life of 570 K cycles at $e_{xx}^{(x,y)}$: 45 % and $e_{yy}^{(x,y)}$: 5 %, (h) stress-strain curves at different time intervals.

to the pink colour region as shown by a black arrow in Fig. 14e, are within 0–0.04. This is quite significant as the maximum strain imposed on the simple square specimen is almost twice with respect to the cruciform sample while the value of the test function is approximately half in the latter compared to the former. The degree of efficiency at maximum global strain of 43 % for the simple square sample can be obtained using equation (10) as follows:

$$\eta_x = \frac{e_{xx}^{FOI}}{e_{xx}^{max}} = \frac{0.43}{0.79} \approx 0.54$$

It can be concluded that the degree of efficiency in the square geometry is three times higher than the cruciform geometry. Considering the test function and the degree of efficiency obtained for the simple square specimen compared to the cruciform geometry, one can say that

the former geometry can be ideal configuration since a larger area of specimen subject to equi-biaxiality instead of a small area (in the case of bulge test). A fatigue life of 34 K was achieved for the simple-square specimen under 43 % EB strain as shown in Fig. 14g while the stress-strain curves of the last 5 cycles are presented in Fig. 14h. The value of stress in Y-direction is relatively higher than X direction as it is in parallel to the mill direction of rubber used. No significant hysteresis can be seen such that it can be a potential material for WECs requiring a relatively low hysteresis in biaxial mode [5].

5.2.2. UB fatigue test

As it was mentioned earlier, one of the typical loading conditions on flexible membranes used in WECs [21] is the UB loading in which approximate strains in longitudinal and transverse directions in the

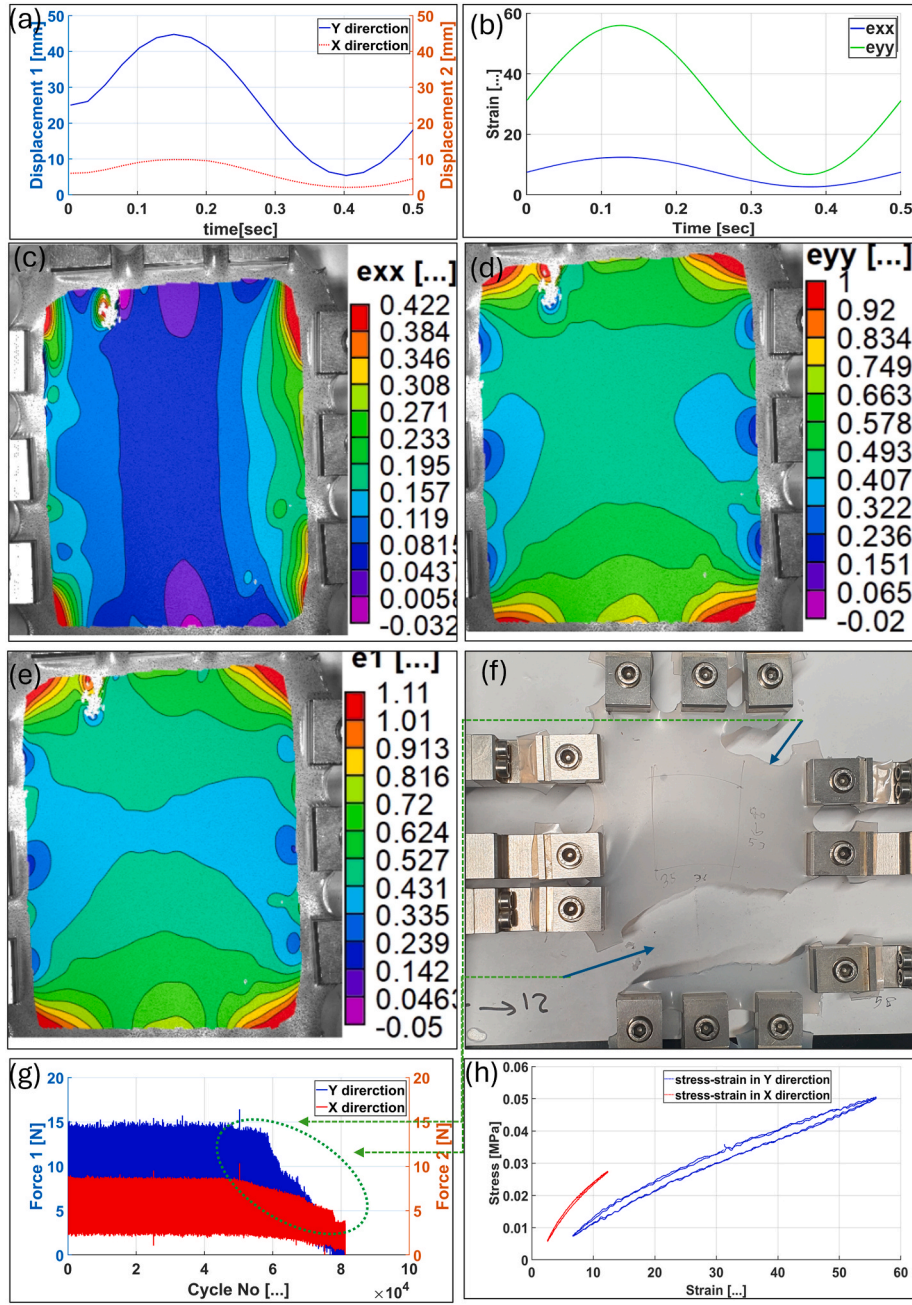


Fig. 16. UB fatigue test conducted on simple-square ecoflex at $e_{xx}^{(x,y)} : 10\%$ and $e_{yy}^{(x,y)} : 55\%$ (a) displacement control test parameters, (b) nominal strains, (c–d) $e_{xx}^{(x,y)}$ and $e_{yy}^{(x,y)}$ distributions, respectively, at the maximum displacement of the machine, (e) maximum principal strain at maximum displacement, (f) fracture surface, (g) Force-cycles No manifesting fatigue life of 76 K cycles, (h) stress strain curves for the first two cycles.

range of 5–10 % and 45–55 %, respectively, are applied to the membrane. Hence, this test is performed to better evaluate fatigue life of NR in a more realistic condition. Fig. 15a illustrates the UB tension fatigue test parameters, i.e., a fixed displacement control was applied whereas the resulting strains, extracted by virtual extensometer, can be seen in Fig. 15b. From Fig. 15a and b, it can be concluded that the strain can be approximately obtained using the displacement of the machine for simplicity (only for simple square geometry). 2D strain fields of the $e_{xx}^{(x,y)}$, $e_{yy}^{(x,y)}$ and e_1 are shown in Fig. 15c–e, respectively, indicating a big area of unequal biaxiality possessing $e_{xx}^{(x,y)} = 5\%$ and $e_{yy}^{(x,y)} = 45\%$ is achieved.

In addition, strain concentration imposed by the grips is also notable where e_1 of 100 % can be seen in the vicinity of corner grips (Fig. 15e).

This indicates that strain near the gripping region is twice the strain in the FOI resulting in a premature failure in the vicinity of the grips during the UB fatigue test as shown in Fig. 15f. Nevertheless, an UB tension fatigue life of 570K cycles is achieved (Fig. 15g). Finally, the stress-strain curves in X and Y directions in the first cycle, cycle No. 520K (few thousand cycles before crack initiation), and cycle No. 571K (few hundred cycles after catastrophic failure) are shown in Fig. 15h. No significant hysteresis can be noted as the applied strain is not high enough, i.e., not in a nonlinear region. Apart from that, the presence of stress reduction can be observed which can be attributed to continuous polymer chain and crosslink breakage during the high cyclic tests [54].

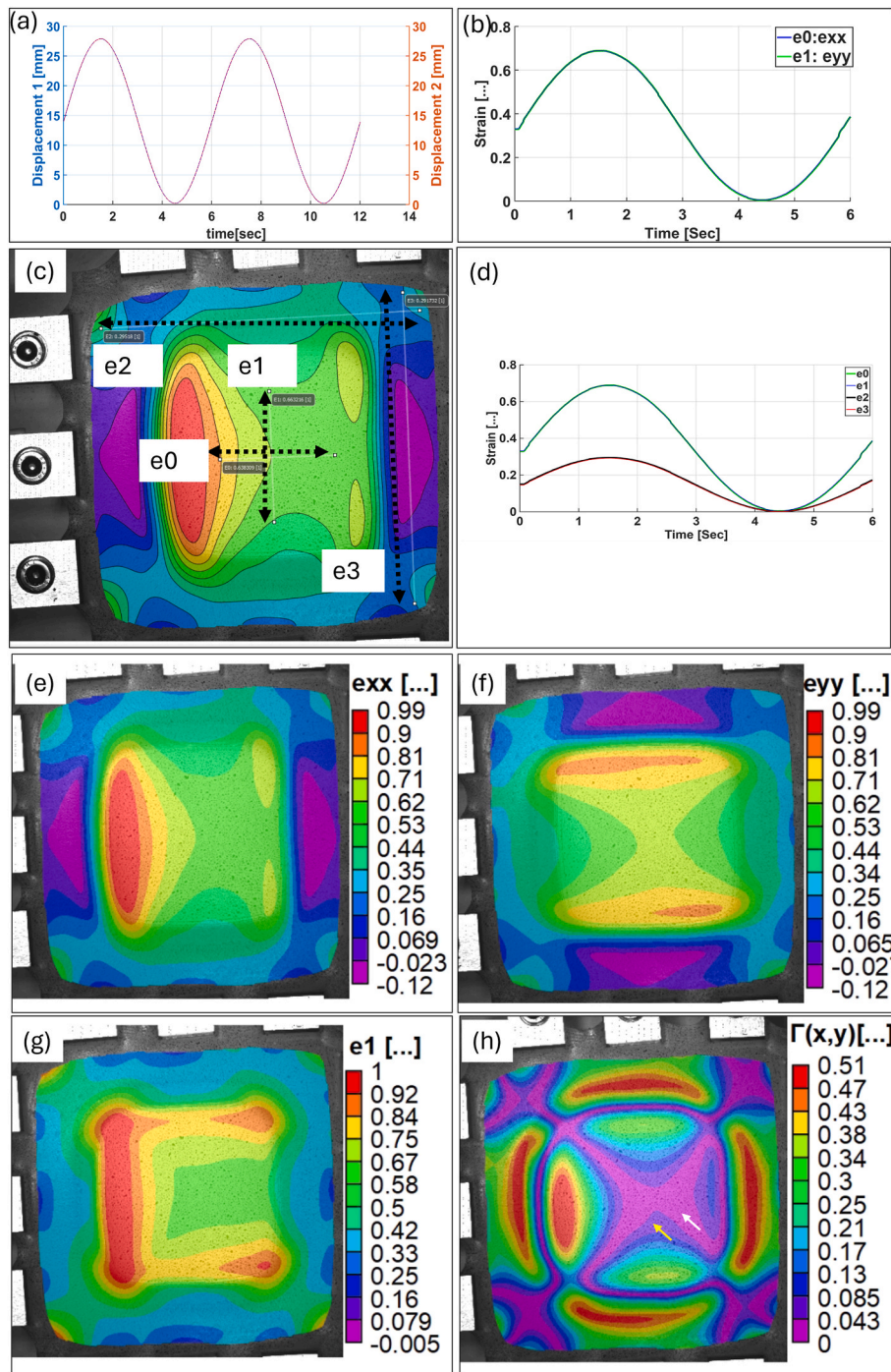


Fig. 17. EB tension characterization at $e_{xx}^{(x,y)} : 65\%$ and $e_{yy}^{(x,y)} : 65\%$ performed on optimized square sample made of ecoflex: (a) displacement control parameters, (b) nominal strains, (c–d) strain comparison in the arm and middle areas showing twice strain in the latter with respect to former, (e–f) $e_{xx}^{(x,y)}$ and $e_{yy}^{(x,y)}$ field, respectively, at the maximum displacement of the machine, (g) maximum principal strain, (h) $\Gamma(x,y)$ at the maximum displacement of the machine.

5.3. Ecoflex

This section starts with UB fatigue performance of ecoflex employing simple square and EB and UB investigation of optimized square specimens. A low frequency EB cyclic test is performed on optimized square geometry to better understand its potential toward standardization of biaxial test.

5.3.1. Simple square specimen: UB fatigue test

Fig. 16a and b shows test setups and the imposed strains in the

central region. The $e_{xx}^{(x,y)}$, $e_{yy}^{(x,y)}$, and $e1$ are presented in Fig. 16c–e, respectively. The strain fields in X and Y directions manifest relatively homogenous distributions in the central region i.e. $e_{xx}^{(x,y)} : 55\%$ and $e_{yy}^{(x,y)} : 10\%$ whereas a maximum strain of 100 % can be seen near the corner grips in the Y direction. This leads to premature failure throughout the fatigue test (Fig. 16f) due to stress concentration imposed to the sample from the grip.

A low fatigue life of 76 K cycles is achieved (Fig. 16g) which is due to lack of edge reinforcement used. Therefore, the gripping region of the

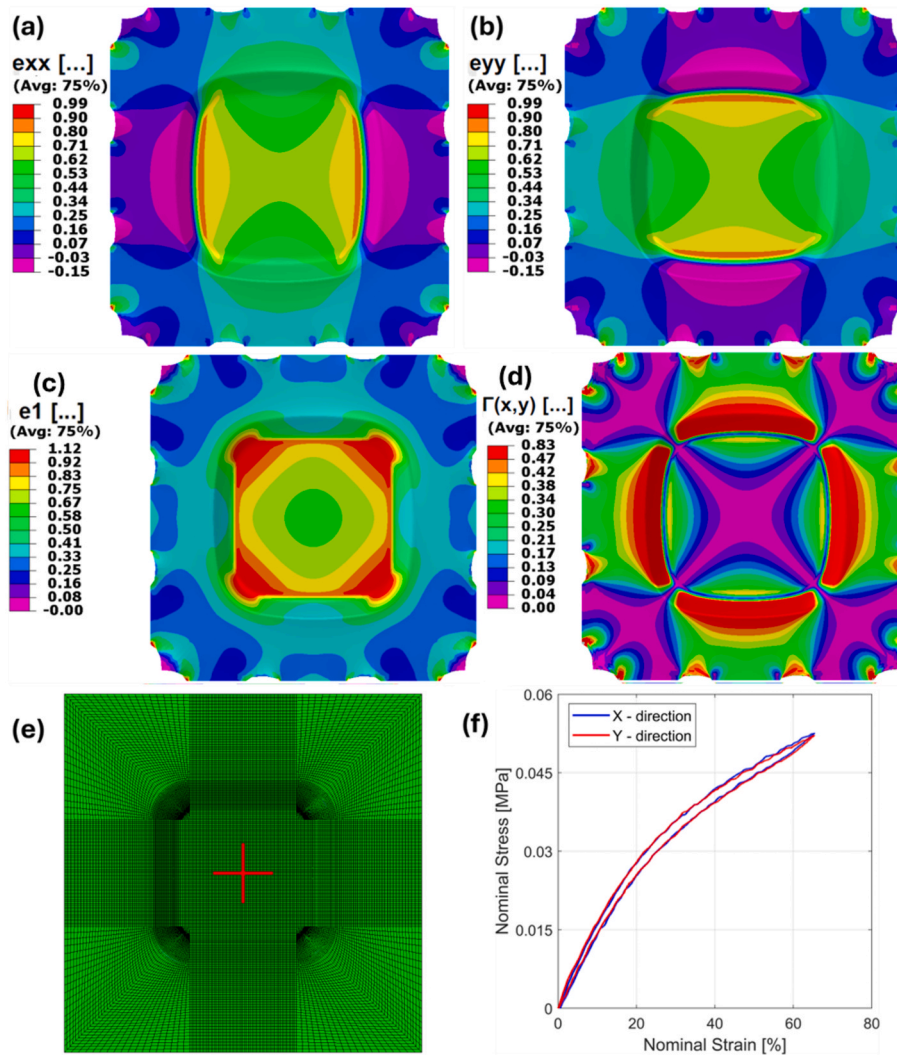


Fig. 18. EB tension results from simulation, (a) nominal strain in X direction (b) nominal strain in Y direction, (c) maximum principal strain, (d) test function $\Gamma(x,y)$, (e) mesh diagram with extensometers in red colour and (f) stress-strain relationship obtained corresponding to the extensometers.

sample should be further reinforced so that a high cyclic biaxial test can be thoroughly achieved. This leads to further optimization of the specimen configuration which will be discussed in the next section. Finally, the stress-strain curves are plotted in Fig. 16h for the first two cycles manifesting large hysteresis which can be related to high shore hardness of the ecoflex used in this study [55].

5.3.2. Optimized square specimen

5.3.2.1. Low frequency EB test. An EB tension test with a low frequency (0.16 Hz) was conducted to better evaluate the performance of the optimized square specimen (Fig. 17). The maximum movement of the machine in both directions were 27.5 mm (Fig. 17a) while maximum strains of 65 % was achieved in the FOI (Fig. 17b). Various virtual extensometers were placed in the samples as shown in Fig. 17c to better distinguish the imposed strains in the FOI and arms (Fig. 17d). It can be concluded that the movement of the machine up to 27.5 mm results in strain values of 65 % and 30 % in the FOI and arms, respectively. Likewise, a maximum strain of 99 % is also notable in the corners of central square cavity (Fig. 17e and f) which can be related to cross-sectional change leading to stress concentration. This can be further validated by the maximum principal strain presented in Fig. 17g. Test functions of $\Gamma(x,y) < 0.04$ and $0.04 < \Gamma(x,y) < 0.08$ are obtained in the central regions as highlighted by white and yellow arrows, respectively,

in Fig. 17h.

The degree of efficiency at the maximum strain can be obtained using equation (10) as follows:

$$\eta_x = \frac{e_{FOI}^{xx}}{e_{max}^{xx}} = \frac{0.65}{0.99} \approx 0.66$$

This demonstrates the highest efficiency amongst all tested geometries in this study while a maximum strain of 65 % in the middle is achieved. It is worth noting that not only the area of equi-biaxiality matters but it is also important to reach a large value of EB strain in the FOI without premature failure or damage evolution caused by gripping in the clamping regions.

The results of simulations are presented in Fig. 18 where a, b and c illustrate the nominal strains in X, Y directions and the principal strain, respectively. While the experimental findings show an asymmetry in the results due to improper gripping conditions, the simulation results illustrated in Fig. 18 demonstrate a perfectly symmetric contours with strain values shown in Fig. 18a, b and c matching closely to experiments especially in the FOI. Now the biaxiality test function $\Gamma(x,y)$ illustrated in Fig. 18d shows a remarkable similarity to that of experiments in the FOI where $\Gamma < 0.08$. The stress-strain curve obtained from the experiment calculated by the method described in Section 3 is illustrated in Fig. 18f.

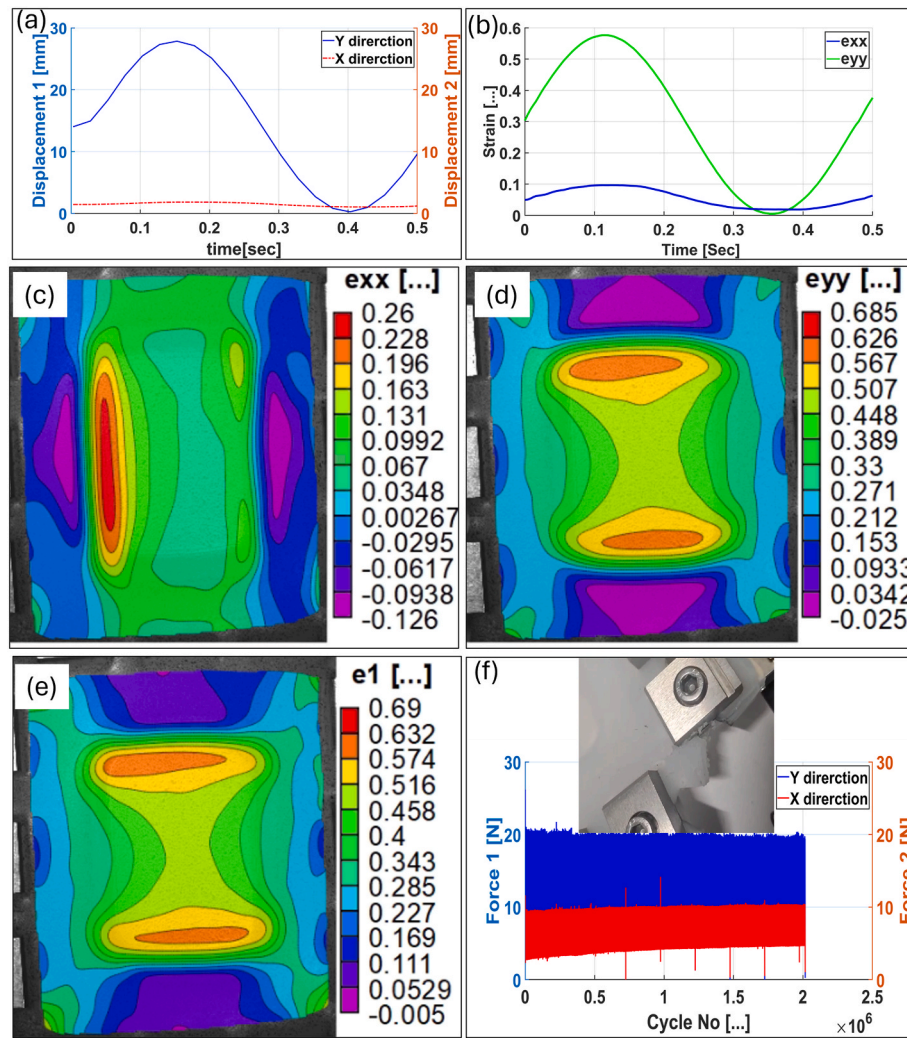


Fig. 19. UB fatigue test on ecoflex at $e_{xx}^{(x,y)}$: 10% and $e_{yy}^{(x,y)}$: 55 %: (a) displacement control parameters, (b) nominal strains, (c–d) $e_{xx}^{(x,y)}$ and $e_{yy}^{(x,y)}$ fields, respectively, at the maximum displacement of the machine, (e) maximum principal strain, (f) high cyclic fatigue test results conducted up to 2 million cycles manifesting crack initiation at corner grips at cycle No > 1.8 million.

Table 4

Comparison of machine displacements and resultant strains in the FOI for square geometry made of ecoflex.

Specimen	DISP- X (mm)	DISP- Y (mm)	$e_{xx}^{(x,y)}$ (%)	$e_{yy}^{(x,y)}$ (%)	Fatigue life (Cycle No)
Simple	10	45	10	55	78,000
Optimized	2.5	27.5	10	55	2,000,000

DISP: Displacement.

5.3.2.2. UB fatigue test. UB tension fatigue on an optimized square geometry was conducted based on the test parameters presented in Fig. 19a while the imposed strains in the FOI extracted by a virtual extensometers is plotted in Fig. 19b. The strain fields, $e_{xx}^{(x,y)}$, $e_{yy}^{(x,y)}$, and e_1 , are illustrated in Fig. 19c–e, respectively. Nominal strains in X and Y directions in the FOI are approximately 55 % and 10 %, respectively, whereas the maximum strains in the arm (the reinforced edge) are around 28 % and 8 %, respectively (Fig. 19c–d). For comparison, the displacement parameters and resulting strains in the FOI for both simple square and optimized square specimens are listed in Table 4. Optimized square geometry can effectively reach much higher strain in the FOI with less movement of the machine while possessing ultra-high biaxial fatigue life (Fig. 19f).

This sheds light on developing reliable and effective test procedure for biaxial fatigue testing of elastomers as no standard and protocol are available. Apart from the significant performance of the optimized square geometry, presence of cracks in the vicinity of the corner grips at cycle numbers >1.8 million is notable as shown in Fig. 19f. This can be attributed to cyclic movement of the grips during fatigue test resulting in damage evolution near the corner grips which possess the highest strain (Fig. 19d and e). It can be concluded that a higher strain can be achieved for the optimized square geometry with a relatively small amount of machine movement whereas further machine displacement is required to achieve the same level of strain for the simple square geometry. It is worth noting that the sample could be further optimized by repositioning the thin section (FOI) to the mid-plane of the thickness, making it symmetric along the thickness direction. However, this modification would require a closed mould, whereas the current design can be produced using an open mould, which greatly simplifies the sample preparation process, time, and cost.

Fig. 20 illustrates the results from simulation of the optimized square geometry under UB condition. Fig. 20a–c illustrates the nominal strains in X and Y directions and the maximum principal strain, respectively. Fig. 20d shows the extensometers in the deformed configuration and marked by red colours. Finally, Fig. 20e shows the stress-strain relationship of the material in UB conditions explained in Fig. 19a and b. A

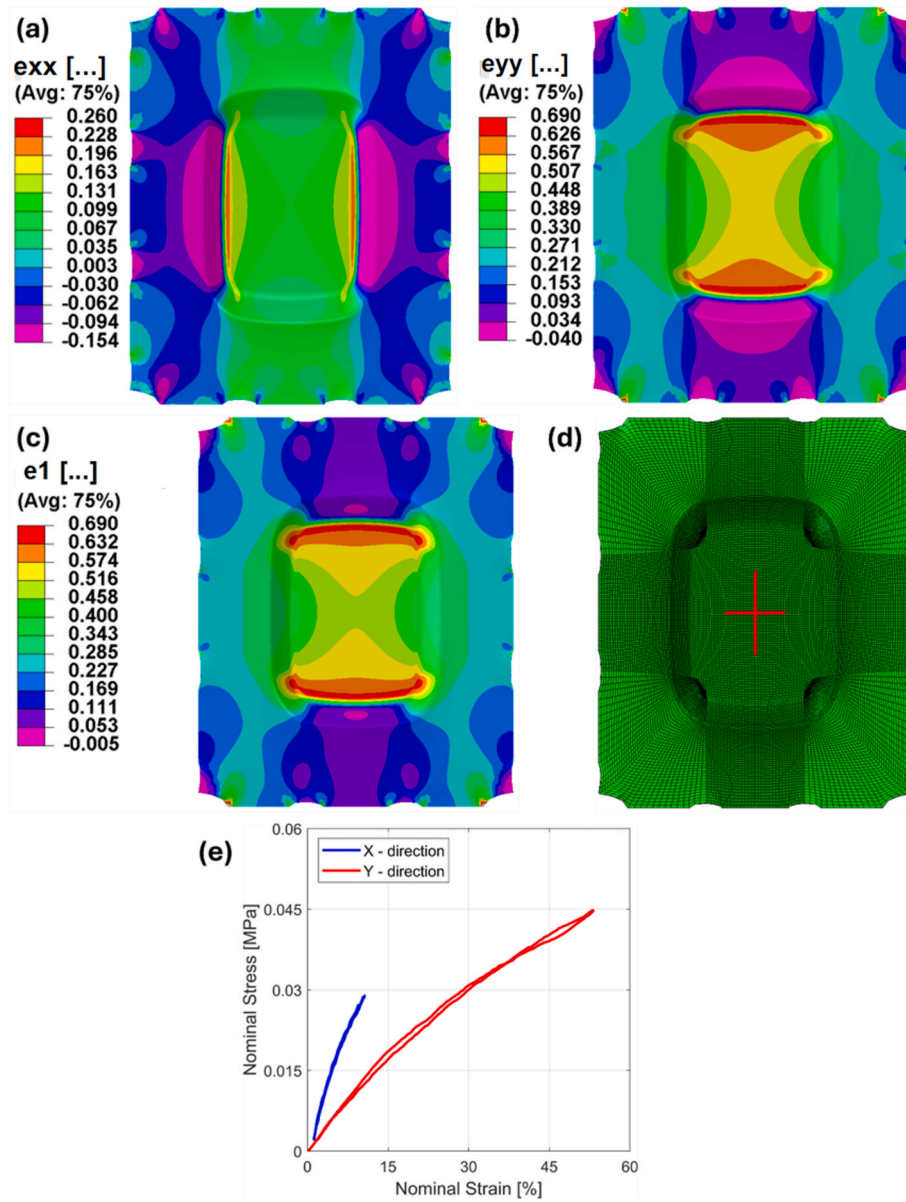


Fig. 20. Simulation results for UB tension test: (a) nominal strain in X direction, (b) nominal strain in Y direction, (c) maximum principal strain, (d) deformed mesh showing the extensometer in red colour, (e) stress-strain curves.

good agreement between simulation results and experiments in terms of nominal and principal strains is achieved verifying the numerical methodology used in this study, thus, the stress-strain curve plotted in Fig. 20e is precisely correct.

6. Comparison and future study

Different test configurations, materials, and biaxial modes including equal and unequal, were conducted in this study. Two parameters were already defined in the literature to find out the degree of biaxiality including test function $\Gamma(x, y)$ and the degree of efficiency η_x . Here, we define a new factor (unitless) which is quite important for the biaxial fatigue test called Strain Ratio (SR) based on equation (11) which indicates the amount of machine displacement required to reach the desired strains in the central region (FOI) with no concern of failure imposed by grips, i.e.,

$$SR_{xx}[\dots] = \frac{e_{xx}^{FOI}[\dots]}{e_{xx}^{gl}[\dots]} \quad (11)$$

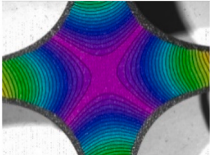
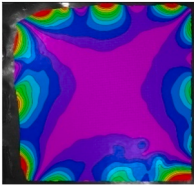
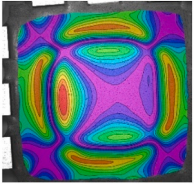
$$E_{xx}^{gl}[\dots] = \frac{\Delta L_{xx}^{max} [mm]}{L_i [mm]} \quad (12)$$

where e_{xx}^{FOI} is the maximum strain in the FOI obtained by DIC, e_{xx}^{gl} is the maximum global strain obtained using equation (12), ΔL_{xx}^{max} is the maximum displacement of the machine, and L_i is the initial grip to grip distance. SR_{yy} can be obtained in the same way due to symmetry.

Regardless of the materials used, the biaxiality criteria for EB tests conducted in this study at $\Gamma(x, y) = 0.04$ are compared in Table 5. It can be concluded that the optimized configuration shows much better performance since e_{xx}^{FOI} , SR, and η , are higher than other geometries.

The optimized square configuration will help to reach higher biaxial tension fatigue life as it reduces the stress concentration in the corner of the central cavity. It is worth noting that fatigue life of any materials is an inherent property of the materials and independent of specimen design or testing method. However, lack of proper specimen geometry in biaxial mode led to premature failure due to stress concentration imposed by the grips as well as improper strain distribution resulting

Table 5
Comparison of equi-biaxiality criteria for different sample geometries in EB mode.

Material	Geometry	ΔL_{max} (mm)	e_{xx}^{gl} (mm)	e_{xx}^{FOI} (mm)	SR (...)	η (...)	$I(x,y) : 0.04$ (...)
NR	Cruciform	35	0.64	0.2	0.31	0.17	
NR	Simple-Square	45	0.49	0.43	0.88	0.54	
Ecoflex	Optimized	27.5	0.33	0.65	1.96	0.66	

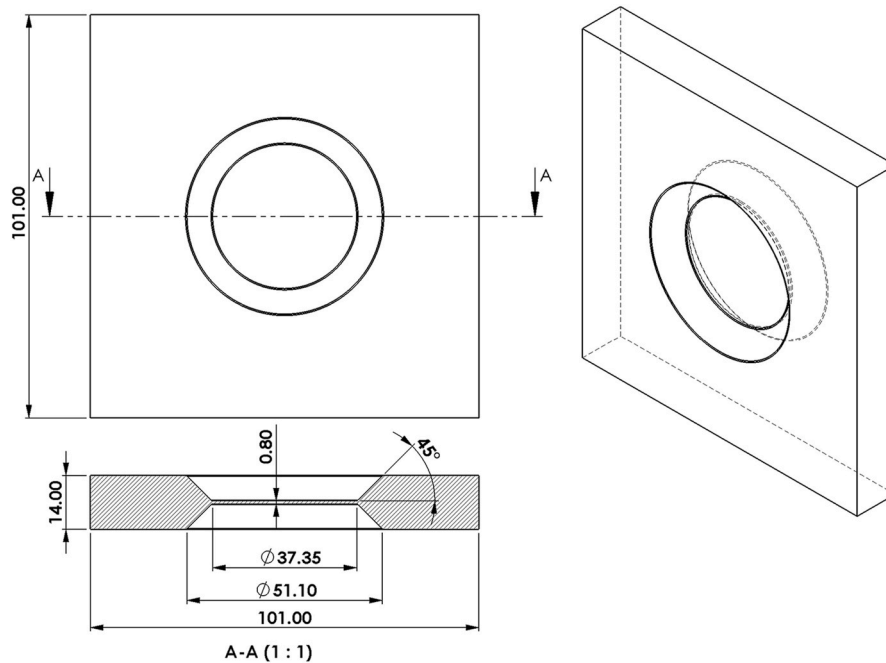


Fig. 21. Recommended optimized square geometry with a circular cavity in the middle.

from poor specimen design. Therefore, it is important to optimize the specimen geometry to avoid aforementioned issues and to reach higher fatigue life while samples can fail from the gauge region not in the vicinity of the grip. We believe that the new geometry can shed more light into performing high cyclic biaxial tension fatigue and therefore fatigue life of the materials can be thoroughly obtained.

Considering the small area of equi-biaxiality in the cruciform geometry, we believe square specimen can be ideal choice in biaxial testing due to much higher efficiency (η) as well as SR with respect to the cruciform sample. In fact, a maximum strain of 43 % can be imposed to the central region of NR simple-square geometry possessing η of 0.54 while a maximum strain of 20 % is reached in the cruciform sample with

small η of 0.17. This clearly indicates significant performance of the simple square geometry with respect to the cruciform in the biaxial mode. We suggest that the geometry of the optimized square specimen could be further improved by replacing the central square cavity with a circular one as shown in Fig. 21. To further illustrate the effectiveness of the new geometry, we resort to the results from simulations.

Firstly, a comparison of the simulation results to that of the Treloar's data is performed and is shown in Fig. 22a. The stress-strain behaviour is nearly identical and is matching closely to that of experiments for all the three cases of extensometer lengths considered $L_G \in [20 \ 28 \ 35]$ mm. This means that the entire circular cavity area undergoes EB deformation unlike the optimized square geometry presented earlier, where a much

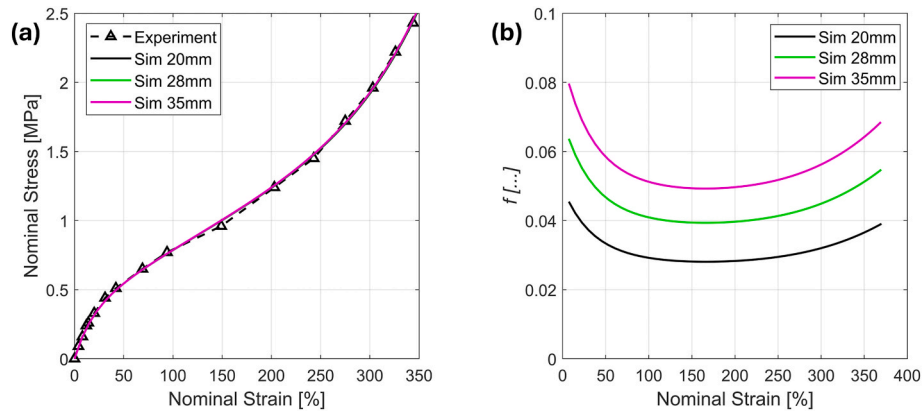


Fig. 22. Simulation results for the optimized square geometry with a circular cavity: (a) comparison of the stress-strain relationship corresponding to different gauge lengths to that of the Treloar's data [43], (b) comparison of the variation of ratio 'f' at different strains corresponding to three different gauge lengths.

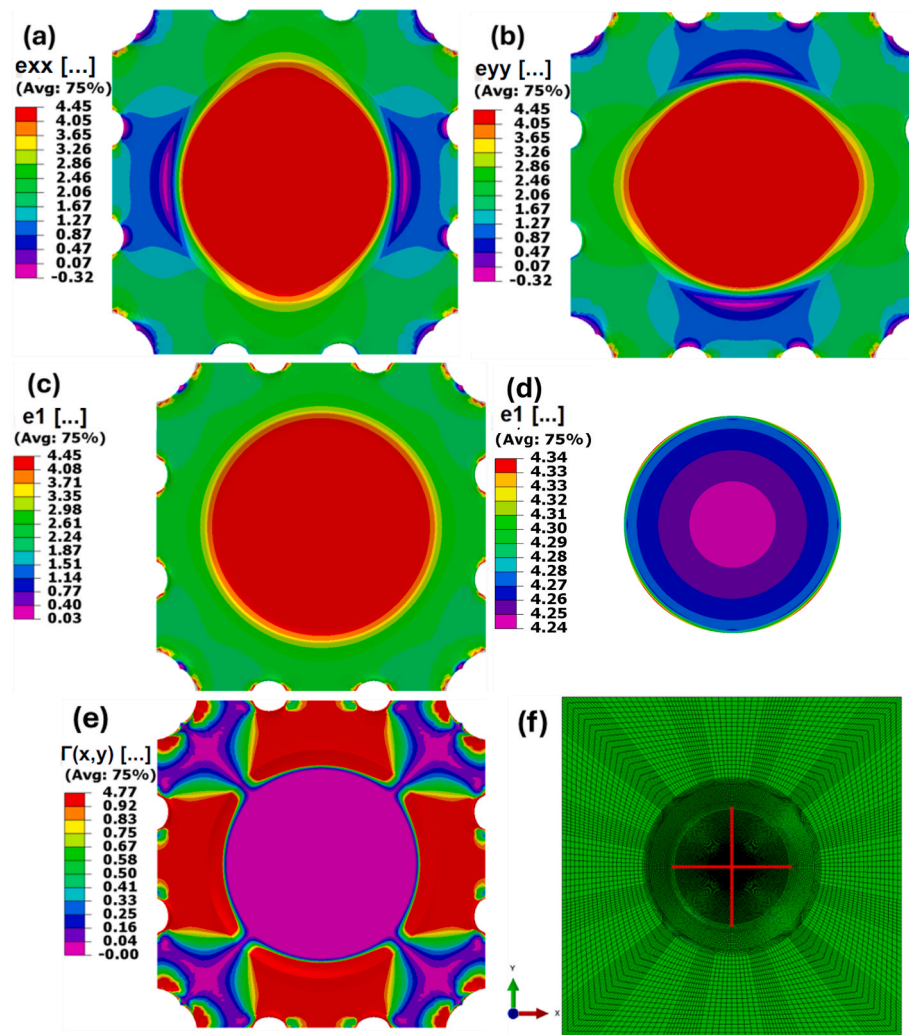


Fig. 23. EB tension results from simulation for the optimized square sample with a circular cavity: (a) nominal strain in X direction (b) nominal strain in Y direction, (c) maximum principal strain, (d) maximum principal strain in the central gauge portion, (e) test function $\Gamma(x,y)$, (f) mesh diagram with 35 mm extensometers shown in red colour.

smaller extensometer was required. Furthermore, the scaling factor 'f' is illustrated in Fig. 22b which can be used for calculating stresses from experimental data.

Fig. 23 further illustrates the results from the simulation where the specimen is deformed by 220 mm in both X and Y directions where

Fig. 23a–b and c show the nominal strains in X, Y directions and the principal strain, respectively. Additionally, Fig. 23d provides the maximum principal strain in the central gauge portion of the sample showing great uniformity having a variation of only 2.3 %. Fig. 23e depicts the spatial variation of the test function $\Gamma(x,y)$. It can be

observed that $\Gamma(x,y)$ is nearly identical for the entire central circular cavity area and satisfies $\Gamma(x,y) < 0.04$ which further illustrates excellent equi-biaxiality of the specimen in the FOI. Hence, the entire area of the circular cavity can be deemed to be effective in the biaxial tension such that stress can be simply obtained from the entire cross-section of the circular region as shown by the extensometer marked in red colour in Fig. 23f. Further, the degree of efficiency at the maximum strain can be obtained using equation (10) as follows:

$$\eta_x = \frac{e_{xx}^{FOI}}{e_{xx}^{max}} = \frac{4.45}{4.45} \approx 1.0$$

Similarly, the SR in either direction can be calculated using equation (11) such that

$$SR_{x,y} = \frac{e_{xy}^{FOI}}{e_{xy}^{gl}} = \frac{4.45}{2.1} = 2.12$$

Thus, both the efficiency η and SR for the proposed section is significantly improved compared to the optimized square geometry with central square cavity and has the potential to yield consistent results from experiments. So, the recommended configuration shown in Fig. 21 can significantly enhance the biaxiality performance and will lead to proper EB fatigue.

7. Conclusion

Various biaxial tension tests were performed on NR and ecoflex while different sample configurations including cruciform, simple square, and optimized square, and test parameters were used to investigate the potential of biaxial tension loading for fatigue testing of elastomers. The following findings were drawn:

- Three criteria were defined to evaluate the equi-biaxiality performance: (i) test function ($\Gamma(x,y)$), or degree of biaxiality showing whether homogeneous strains can be achieved in the FOI, (ii) degree of efficiency (η) manifesting the ratio of strain in the FOI to maximum strain in the samples apart from the FOI which can highlight the importance of gripping and gauge-section reduction to avoid premature failure near the gripping regions, (iii) SR which is an important factor especially for fatigue test. SR indicated that how much machine movement was required to reach the desired strain in the FOI. It was concluded that a good equi-biaxiality can be obtained at test function in the range of 0.04.
- Cruciform geometry showed least performance in the equi-biaxiality criteria possessing η_x : 0.17 at EB strain of 20 % in the FOI whereas the NR-simple square geometry could reach to η_x and e_{xx}^{FOI} as high as 0.54 and 43 %, respectively. The highest equi-biaxiality performance was obtained for the optimized square geometry, i.e., e_{xx}^{FOI} : 65% and η_x of 0.66 were achieved.
- The highest SR was achieved for the optimized square specimen followed by the simple square whereas the cruciform specimen showed lowest values. It was concluded that the optimized geometry can effectively reach much higher strain in the FOI with remarkably less movement of the machine (higher SR) and less strain near the grip (higher η) while possessing ultra-high biaxial fatigue life (~1.8 million cycles).
- EB fatigue test conducted on cruciform samples made of NR manifested a very low fatigue life of 270 K cycles at strain of 20 % which failed from the grips. This was attributed to its weak degree of efficiency thus gripping effect was significant in the cruciform specimen without any arm reinforcement.
- UB tension fatigue test was conducted on ecoflex to measure fatigue life in such a way that approximately 10 % and 55 % strains can be applied on in X and Y directions to mimic service condition of flexible membrane used in WECs. It was shown that optimized sample could

reach of 2 million fatigue cycles while crack near the grip was initiated at around 1.8 million cycles.

- A new test configuration was recommended for future study i.e., a square sample with a circular cavity in the middle. The preliminary studies with the help of simulations shows nearly uniform strain distribution in the entire circular cavity area leading to a larger area of equi-biaxiality and consequently a larger FOI. Further the numerical study yielded an efficiency value η of 1 and SR value of 2.12 showing a potential for considerable improvements over the cruciform and the optimized square geometries.

CRedit authorship contribution statement

Ali Esmaeili: Writing – original draft, Investigation, Formal analysis, Conceptualization. **Deepak George:** Writing – original draft, Investigation, Formal analysis. **Lewis Tunncliffe:** Writing – review & editing, Funding acquisition. **Ian Masters:** Writing – review & editing, Supervision. **Mokarram Hossain:** Writing – review & editing, Supervision, Funding acquisition, Conceptualization.

Declaration of competing interest

The authors declare that they have no known competing financial interests or personal relationships that could have appeared to influence the work reported in this paper.

Acknowledgements

This study is funded by the Swansea Bay City Deal and the European Regional Development Fund through the Welsh European Funding Office. This study is also supported by EPSRC through the Supergen ORE Hub (EP/S000747/1), who have awarded funding for the Flexible Fund project Submerged biaxial fatigue analysis for Flexible membrane Wave Energy Converters (FF2021-1036). A. Esmaeili and M. Hossain acknowledge financial support from Birla Carbon, USA to facilitate parts of this study. We would like to thank the access to characterization equipment to Swansea University Advanced Imaging of Materials (AIM) facility, which was funded in part by the EPSRC (EP/M028267/1) and the European Regional Development Fund through the Welsh Government (80708). M. H. also acknowledges the support from the Engineering and Physical Sciences Research Council (EPSRC) under the grant (EP/Z535710/1).

Appendix A. Supplementary data

Supplementary data to this article can be found online at <https://doi.org/10.1016/j.polymertesting.2025.109060>.

Data availability

Data will be made available on request.

References

- [1] Y.L. Tee, M.S. Loo, A. Andriyana, Recent advances on fatigue of rubber after the literature survey by Mars and fatemi in 2002 and 2004, *Int. J. Fatig.* 110 (2018) 115–129, <https://doi.org/10.1016/j.ijfatigue.2018.01.007>.
- [2] A. Esmaeili, D. George, T. Lake, L. Tunncliffe, I. Masters, M. Hossain, The importance of rubber compounding approach in damage evolution and fatigue performance of carbon nanotubes doped natural rubber, *Fatig. Fract. Eng. Mater. Struct.* (2025), <https://doi.org/10.1111/ffe.70065>.
- [3] Z. Liu, Z. Zhang, R.O. Ritchie, Structural orientation and anisotropy in biological materials: functional designs and mechanics, *Adv. Funct. Mater.* 30 (2020), <https://doi.org/10.1002/adfm.201908121>.
- [4] I. Denora, C. Marano, Stretch-induced softening in filled elastomers: a review on mullins effect related anisotropy and thermally induced recovery, *Polym. Test.* 133 (2024), <https://doi.org/10.1016/j.polymertesting.2024.108399>.
- [5] I. Collins, M. Hossain, W. Dettmer, I. Masters, Flexible membrane structures for wave energy harvesting: a review of the developments, materials and

- computational modelling approaches, *Renew. Sustain. Energy Rev.* 151 (2021) 111478, <https://doi.org/10.1016/j.rser.2021.111478>.
- [6] F. Abad, S. Lotfian, S. Dai, G. Zhao, G.I. Alarcon, L. Yang, Y. Huang, Q. Xiao, F. Brennan, Experimental and computational analysis of elastomer membranes used in oscillating water column WECs, *Renew. Energy* 226 (2024) 120422, <https://doi.org/10.1016/j.renene.2024.120422>.
 - [7] D. George, I. Collins, I. Masters, M. Hossain, Extreme load analysis of flexible wave energy converters utilising nonlocal continuum damage mechanics, *Appl. Ocean Res.* 142 (2024), <https://doi.org/10.1016/j.apor.2023.103843>.
 - [8] X. Hu, H. Zhu, S. Chen, H. Yu, S. Qu, Magnetomechanical behavior of soft magnetoactive membranes, *Int. J. Solid Struct.* (2022) 111310, <https://doi.org/10.1016/j.ijsolstr.2021.111310>, 234–235.
 - [9] D. Gorman, N. Murphy, R. Ekins, S. Jerrams, The evaluation of the effect of strain limits on the physical properties of magnetorheological elastomers subjected to uniaxial and biaxial cyclic testing, *Int. J. Fatig.* 103 (2017) 1–4, <https://doi.org/10.1016/j.ijfatigue.2017.05.011>.
 - [10] Y. Zhou, L. Jiang, S. Chen, J. Ma, A. Betts, S. Jerrams, Determination of reliable fatigue life predictors for magnetorheological elastomers under dynamic equibiaxial loading, *Polym. Test.* 61 (2017) 177–184, <https://doi.org/10.1016/j.polymertesting.2017.05.021>.
 - [11] T. Lu, C. Ma, T. Wang, Mechanics of dielectric elastomer structures: a review, *Extreme Mech Lett* 38 (2020) 100752, <https://doi.org/10.1016/j.eml.2020.100752>.
 - [12] A. Esmaili, D. George, I. Masters, M. Hossain, Biaxial experimental characterizations of soft polymers: a review, *Polym. Test.* 128 (2023) 108246, <https://doi.org/10.1016/j.polymertesting.2023.108246>.
 - [13] M. Johnson, N. Murphy, R. Ekins, J. Hanley, S. Jerrams, Equi-biaxial fatigue testing of EPM utilising bubble inflation, *Polym. Test.* 53 (2016) 122–131, <https://doi.org/10.1016/j.polymertesting.2016.05.017>.
 - [14] Y. Zhou, S. Jerrams, L. Chen, Multi-axial fatigue in magnetorheological elastomers using bubble inflation, *Mater. Des.* 50 (2013) 68–71, <https://doi.org/10.1016/j.matdes.2013.02.071>.
 - [15] F. Lo Savio, G. La Rosa, M. Bonfanti, A new theoretical-experimental model deriving from the contactless measurement of the thickness of bulge-tested elastomeric samples, *Polym. Test.* 87 (2020) 106548, <https://doi.org/10.1016/j.polymertesting.2020.106548>.
 - [16] J.Y. Sheng, L.Y. Zhang, B. Li, G.F. Wang, X.Q. Feng, Bulge test method for measuring the hyperelastic parameters of soft membranes, *Acta Mech.* 228 (2017) 4187–4197, <https://doi.org/10.1007/s00707-017-1945-x>.
 - [17] U.D. Çakmak, I. Kallaf, Z. Major, Temperature dependent bulge test for elastomers, *Mech. Res. Commun.* 60 (2014) 27–32, <https://doi.org/10.1016/j.mechrescom.2014.05.006>.
 - [18] V. Anand, S.C. Muchandimath, I.C. Christov, Hydrodynamic bulge testing: materials characterization without measuring deformation, *Journal of Applied Mechanics*, Transactions ASME 87 (2020), <https://doi.org/10.1115/1.4046297>.
 - [19] Sam Leighton, Campbell Algie, Wave energy conversion/convertors, AU, Bentley (AU). Shawn Kay Ryan, 2021. <https://patentimages.storage.googleapis.com/fc/cc/fb/9cd335c733c362/US10883471.pdf>.
 - [20] A. Bombora, Patented membrane-style Wave Energy Converter, mWaveTM, 2020. <https://bomborawave.com/mwave/>.
 - [21] A. Babarit, G. Benjamin, J. Singh, C. Mélis, A. Babarit, G. Benjamin, J. Singh, C. Mélis, P.J. Hydro-elastic, B. Gendron, Hydro-Elastic Modelling of an electro-active Wave Energy Converter to Cite This Version : HAL Id : Hal-01201934, 2019.
 - [22] T. Shi, J. Hu, W. Chen, C. Gao, Biaxial tensile behavior and strength of architectural fabric membranes, *Polym. Test.* 82 (2020), <https://doi.org/10.1016/j.polymertesting.2019.106230>.
 - [23] T. Shi, W. Chen, C. Gao, J. Hu, B. Zhao, P. Wang, M. Wang, Biaxial strength determination of woven fabric composite for airship structural envelope based on novel specimens, *Compos. Struct.* 184 (2018) 1126–1136, <https://doi.org/10.1016/j.compstruct.2017.10.067>.
 - [24] L. Chen, W. Chen, C. Gao, S. Li, Y. Song, H. Zhao, J. Hu, B. Zhao, Strength analysis of composite envelope structures considering the tension–shear coupling and cutting pattern effect, *Thin-Walled Struct.* 180 (2022), <https://doi.org/10.1016/j.tws.2022.109919>.
 - [25] L. Chen, W. Chen, A rationalized macroscopic failure criterion of composite woven fabrics for airship structures, *Thin-Walled Struct.* 206 (2025), <https://doi.org/10.1016/j.tws.2024.112647>.
 - [26] H. Seibert, T. Scheffer, S. Diebels, Biaxial testing of elastomers - experimental setup, measurement and experimental optimisation of specimen's shape, *Tech. Mech.* 34 (2014) 72–89, <https://doi.org/10.24352/UB.OVGU-2017-054>.
 - [27] K.B. Putra, X. Tian, J. Plott, A. Shih, Biaxial test and hyperelastic material models of silicone elastomer fabricated by extrusion-based additive manufacturing for wearable biomedical devices, *J. Mech. Behav. Biomed. Mater.* 107 (2020) 103733, <https://doi.org/10.1016/j.jmbbm.2020.103733>.
 - [28] L.M. Palacios-Pineda, I.A. Perales-Martínez, M.R. Moreno-Guerra, A. Elías-Zúñiga, An optimum specimen geometry for equibiaxial experimental tests of reinforced magnetorheological elastomers with iron micro- and nanoparticles, *Nanomaterials* 7 (2017), <https://doi.org/10.3390/nano7090254>.
 - [29] M. Jiang, Z. Wang, A.D. Freed, M.R. Moreno, V. Erel, A. Dubrowski, Extracting material parameters of silicone elastomers under biaxial tensile tests using virtual fields method and investigating the effect of missing deformation data close to specimen edges on parameter identification, *Mech. Adv. Mater. Struct.* 29 (2022) 6421–6435, <https://doi.org/10.1080/15376494.2021.1979138>.
 - [30] T.T. Mai, K. Urayama, Biaxial loading effects on strain energy release rate and crack-tip strain field in elastic hydrogels, *Macromolecules* 54 (2021) 4792–4801, <https://doi.org/10.1021/acs.macromol.1c00445>.
 - [31] J. Li, D. Xiang, P. Su, C. Zhao, H. Li, Z. Li, B. Wang, P. Wang, Y. Li, Y. Wu, High-performance flexible strain sensors prepared by biaxially stretching conductive polymer composites with a double-layer structure, *Mater. Today Commun.* 36 (2023) 106548, <https://doi.org/10.1016/j.mtcomm.2023.106548>.
 - [32] X. Zhao, Z.C. Berwick, J.F. Krieger, H. Chen, S. Chambers, G.S. Kassab, Novel design of cruciform specimens for planar biaxial testing of soft materials, *Exp. Mech.* 54 (2014) 343–356, <https://doi.org/10.1007/s11340-013-9808-4>.
 - [33] D. Nozaki, T.-T. Mai, K. Tsunoda, K. Urayama, Tracking the evolution of heterogeneous crystallization driven by complex deformation scenarios in natural rubber, *Macromolecules* (2025), <https://doi.org/10.1021/acs.macromol.5c00160>.
 - [34] M.A. Moreno-Mateos, S. Wiesheier, A. Esmaili, M. Hossain, P. Steinmann, Biaxial characterization of soft elastomers: experiments and data-adaptive configurational forces for fracture, *Journal of the Mechanics and Physics of Solids Journal Homepage* (2025), <https://doi.org/10.5281/zenodo.1>.
 - [35] Y. Zhou, S. Jerrams, A. Betts, G. Farrell, L. Chen, The influence of particle content on the equi-biaxial fatigue behaviour of magnetorheological elastomers, *Mater. Des.* 67 (2015) 398–404, <https://doi.org/10.1016/j.matdes.2014.11.056>.
 - [36] M. Johnson, N. Murphy, R. Ekins, J. Hanley, S. Jerrams, Equi-biaxial fatigue testing of EPM utilising bubble inflation, *Polym. Test.* 53 (2016) 122–131, <https://doi.org/10.1016/j.polymertesting.2016.05.017>.
 - [37] S. Jerrams, N. Murphy, J. Hanley, The significance of equi-biaxial bubble inflation in determining elastomeric fatigue properties. *Advanced Elastomers - Technology, Properties and Applications*, 2012, <https://doi.org/10.5772/50099>.
 - [38] A. Esmaili, I. Masters, M. Hossain, A novel carbon nanotubes doped natural rubber nanocomposite with balanced dynamic shear properties and energy dissipation for wave energy applications, *Results Mater.* 17 (2023) 100358, <https://doi.org/10.1016/j.rinma.2022.100358>.
 - [39] A. Esmaili, I. Masters, M. Hossain, A novel carbon nanotubes doped natural rubber nanocomposite with balanced dynamic shear properties and energy dissipation for wave energy applications, *Results Mater.* 17 (2023) 100358, <https://doi.org/10.1016/j.rinma.2022.100358>.
 - [40] R. Ranjan, H. Murthy, D. Bhowmik, V.S. Sadavarte, Behaviour of composite solid propellant under biaxial tensile loading, *Polym. Test.* 124 (2023) 108054, <https://doi.org/10.1016/j.polymertesting.2023.108054>.
 - [41] E. Lamkanfi, W. Van Paepegem, J. Degrieck, Shape optimization of a cruciform geometry for biaxial testing of polymers, *Polym. Test.* 41 (2015) 7–16, <https://doi.org/10.1016/j.polymertesting.2014.09.016>.
 - [42] W.V. Mars, A. Fatemi, Fatigue crack nucleation and growth in filled natural rubber, *Fatig. Fract. Eng. Mater. Struct.* 26 (2003) 779–789, <https://doi.org/10.1046/j.1460-2695.2003.00678.x>.
 - [43] L.R.G. Treloar, Stress-strain data for vulcanised rubber under various types of deformation, *Trans. Faraday Soc.* 40 (1944) 59–70, <https://doi.org/10.1039/TF9444000059>.
 - [44] M.M. Carroll, A strain energy function for vulcanised rubbers, *J. Elasticity* 103 (2011) 173–187, <https://doi.org/10.1007/s10659-010-9279-0>.
 - [45] P. Steinmann, M. Hossain, G. Possart, Hyperelastic models for rubber-like materials: consistent tangent operators and suitability for Treloar's data, *Arch. Appl. Mech.* 82 (2012) 1183–1217, <https://doi.org/10.1007/s00419-012-0610-z>.
 - [46] C. Kadapa, M. Hossain, A linearized consistent mixed displacement-pressure formulation for hyperelasticity, *Mech. Adv. Mater. Struct.* 29 (2022) 267–284, <https://doi.org/10.1080/15376494.2020.1762952>.
 - [47] ABAQUS/Standard User's Manual, Version 2022, Dassault Systèmes Simulia Corp, United States, 2025 n.d.
 - [48] M.C. Serna Moreno, S. Horta Muñoz, Experimental evaluation of the use of cruciform specimens for biaxial stability analysis, *Compos. B Eng.* 286 (2024), <https://doi.org/10.1016/j.compositesb.2024.111764>.
 - [49] Q. Zhang, L. Liu, L. Zhang, F. Li, How to effectively perform equibiaxial tension for rubber materials? *Polymer (Guildf.)* 324 (2025) 128256 <https://doi.org/10.1016/j.polymer.2025.128256>.
 - [50] T. Shi, W. Chen, C. Gao, J. Hu, B. Zhao, P. Wang, M. Wang, Biaxial constitutive relationship and strength criterion of composite fabric for airship structures, *Compos. Struct.* 214 (2019) 379–389, <https://doi.org/10.1016/j.compstruct.2019.02.028>.
 - [51] R. Ranjan, H. Murthy, D. Bhowmik, V.S. Sadavarte, Behaviour of composite solid propellant under biaxial tensile loading, *Polym. Test.* 124 (2023) 108054, <https://doi.org/10.1016/j.polymertesting.2023.108054>.
 - [52] A. Esmaili, D. George, I. Masters, M. Hossain, Biaxial experimental characterizations of soft polymers: a review, *Polym. Test.* 128 (2023) 108246, <https://doi.org/10.1016/j.polymertesting.2023.108246>.
 - [53] R. Of, T. Draft, A.R.E. Invited, W.T. Comments, O.F. Any, R. Patent, R. Of, T.A.R.E. Aware, I.N. Addition, T.O. Their, E. As, B. Acceptable, F.O.R. Industrial, U. Purposes, D. International, S. May, O. Have, T.O. Be, C. In, D. To, W. Reference, M. A.Y. Be, M. DRAFT INTERNATIONAL STANDARD ISO/FDIS Metallic Materials — Sheet and Strip — Biaxial Tensile Testing Method Using a Cruciform Test Piece Iteb STANDARD PREVIEW Iteb STANDARD PREVIEW, 2021, 2021.
 - [54] L.C. Tang, L. Zhao, F. Qiang, Q. Wu, L.X. Gong, J.P. Peng, Mechanical Properties of Rubber Nanocomposites Containing Carbon Nanofillers, Elsevier Inc., 2019, <https://doi.org/10.1016/B978-0-12-817342-8.00012-3>.
 - [55] Z. Liao, M. Hossain, X. Yao, Ecoflex polymer of different shore hardnesses: experimental investigations and constitutive modelling, *Mech. Mater.* 144 (2020), <https://doi.org/10.1016/j.mechmat.2020.103366>.